TASK QUARTERLY 6 No 1 (2002), 143–176

A PRECONDITIONED SOLUTION SCHEME FOR THE COMPUTATION OF COMPRESSIBLE FLOW IN TURBOMACHINERY AT ARBITRARY MACH NUMBERS

JAN E. ANKER, JÜRGEN F. MAYER AND HEINZ STETTER

Institut für Thermische Strömungsmaschinen und Maschinenlaboratorium,
University of Stuttgart,
Pfaffenwaldring 6, D-70550 Stuttgart, Germany
mayer@itsm.uni-stuttgart.de

(Received 10 August 2001; revised manuscript received 28 December 2001)

Abstract: A preconditioned solution scheme for the computation of compressible flow in turbomachinery at arbitrary Mach numbers is presented. The preconditioning technique used is applied to a state-of-the-art explicit, time-marching Navier-Stokes code which originally was developed for compressible, high-speed turbomachinery applications. It combines the ideas of low Mach number preconditioning and artificial compressibility method into a unified approach where principally fluids with arbitrary equations of state can be simulated. As shown by the test cases presented, it allows the code to simulate flows efficiently and accurately independent of the Mach number. A description of the Navier-Stokes equations for rotating coordinate systems, along with the solution scheme and the details of the preconditioning method is given.

Since turbomachinery computations are often performed on truncated domains, the solution scheme should be used in conjunction with non-reflecting boundary conditions. A change in the time-dependency of the equations due to preconditioning necessitates a modification of the boundary conditions. Thus, a derivation of the appropriate boundary conditions for the presented preconditioned scheme was performed and the resultant equations are given in this paper. The effectiveness of the new boundary conditions is demonstrated by comparing them with both boundary conditions that use the standard one-dimensional characteristic approach and the original boundary conditions for the non-preconditioned case.

Keywords: preconditioning, non-reflecting boundary condition, Mach number independency, turbomachinery flow

1. Introduction

The flow field encountered in turbomachinery is one of the most complicated in fluid dynamics practice. The flow may be incompressible, subsonic, transonic, or supersonic. Many aircraft engines have mixed flows, in which all of these regimes are present in a single blade row [1]. For this reason it would be desirable to have a Navier-Stokes solver which is capable of simulating flow in turbomachinery accurately and efficiently over a broad Mach number and Reynolds number range.

Historically, low speed flows were first solved using solution schemes that solve the Euler or Navier-Stokes equations for incompressible fluids. In the pseudo-compressibility approach introduced by Chorin [2], a pressure time derivative is introduced into the continuity equation, which makes the system of incompressible Navier-Stokes equations hyperbolic and provides a means of updating the pressure in the momentum equations. Alternatively, in the frequently applied pressure-based methods [3], the momentum equations are solved initially with an assumed pressure field, which is continuously updated using an auxiliary elliptic pressure equation.

Since the time-dependent compressible Euler equations are hyperbolic, regardless whether the flow is subsonic or supersonic, density-based time-marching schemes were developed in the context of transonic, external aerodynamic applications [4, 5] and later extended to viscous, internal turbomachinery applications by [6, 7] among others. These methods proved to be very effective for the computation of high Reynolds number flows in the transonic and supersonic regimes. However, these schemes become inefficient and inaccurate at low Mach numbers. For this reason, the computation of low Mach number flow was dominated by solution procedures solving the incompressible Navier-Stokes equations for many years.

The application of time-marching methods could be extended to low Mach number compressible flow after it was realized that the difficulty in solving the compressible equations for low Mach number flow was attributed to the large disparity of the acoustic wave speed and the waves convected at particle speed. Low Mach number perturbation methods were first used to alleviate these problems and were used to calculate low speed compressible flow [8, 9].

In recent years, local preconditioning procedures in which the time derivatives of the compressible Euler and Navier-Stokes equations are altered to control the eigenvalues and to accelerate convergence [10–13] were developed. The destroyed time accuracy is thereby of no restriction: In the limit of a converged solution, the time derivatives disappear wherefore the changed dynamics of the equations do not impair accuracy. When unsteady simulations are to be performed, the preconditioning method must be incorporated into a dual time-stepping scheme, where preconditioning is applied at the inner pseudo-time level, thereby not affecting the outer loop stepping through physical time [13]. Since the preconditioned Navier-Stokes equations are valid at all speeds, they have potential for providing uniform convergence over all Reynolds and Mach number regimes as demonstrated in [14, 15].

In this paper, a preconditioning technique is applied to an explicit, time-marching code which originally was developed for the simulation of compressible, high-speed turbomachinery applications by Merz *et al.* [16] and Jung *et al.* [17]. The presented preconditioning technique for viscous, turbulent flow is based on [13, 15, 18] since this preconditioning method combines the ideas of low Mach number preconditioning and artificial compressibility method into a unified approach. In Chapter 2 the governing equations are described, whereas in Chapter 3 the preconditioning method used is reviewed. The solution scheme and the necessary changes of the original scheme due to preconditioning is described in Chapter 4. Even though the code was only applied to test cases where the fluid was treated as an ideal gas, we follow [19] and present a scheme which enables the simulation of fluids with arbitrary equations of state.

Since turbomachinery computations often are performed on truncated domains, the solution scheme should be used in conjunction with non-reflecting boundary conditions in order to prevent spurious reflections at the interfaces. In the original scheme, at the inlet and exit boundaries as well as at boundaries between different frames of reference in the case of steady-state flow interaction of two blade rows, a non-reflecting post-correction method based on the work of [20, 21] is applied. Obviously, a change in the time-dependent equations also changes the characteristics of the system which necessitates a modification of the original boundary conditions. A derivation of the appropriate boundary conditions for the presented preconditioned scheme was performed for general equations of state. The resultant equations and the main aspects of the novel boundary treatment derived and implemented in our code are given in Chapter 5.

In Chapter 6 we present several test cases in order to demonstrate that preconditioning not only increases accuracy, but also provides convergence rates independent of the Mach number. Finally, the effectiveness of the new boundary conditions is demonstrated by comparing results obtained with these boundary conditions with results gained using boundary conditions for the non-preconditioned case.

2. Governing equations

The flow solver ITSM3D uses the fully three-dimensional, unsteady Favre-averaged Navier-Stokes equations

$$\frac{\partial \mathbf{Q}}{\partial t}+\frac{\partial(\mathbf{E}_c-\mathbf{E}_v)}{\partial x}+\frac{1}{r}\frac{\partial(\mathbf{F}_c-\mathbf{F}_v)}{\partial \phi}+\frac{1}{r}\frac{\partial[r(\mathbf{G}_c-\mathbf{G}_v)]}{\partial r}=\mathbf{H}_c-\mathbf{H}_v \tag{1}$$

with

$$\mathbf{Q}=\begin{pmatrix}\varrho\\ \varrho v_x\\ \varrho v_\phi\\ \varrho v_r\\ \varrho e_0\end{pmatrix},\quad \mathbf{E}_c=\begin{pmatrix}\varrho v_x\\ \varrho v_x^2+p\\ \varrho v_x v_\phi\\ \varrho v_x v_r\\ \varrho h_0 v_x\end{pmatrix},\quad \mathbf{E}_v=\begin{pmatrix}0\\ \tau_{xx}\\ \tau_{x\phi}\\ \tau_{xr}\\ \tau_{xi}v_i+k\frac{\partial T}{\partial x}\end{pmatrix},\quad \mathbf{F}_c=\begin{pmatrix}\varrho v_\phi\\ \varrho v_\phi v_x\\ \varrho v_\phi^2+p\\ \varrho v_\phi v_r\\ \varrho h_0 v_\phi\end{pmatrix},$$

$$\mathbf{F}_v=\begin{pmatrix}0\\ \tau_{\phi x}\\ \tau_{\phi\phi}\\ \tau_{\phi r}\\ \tau_{\phi i}v_i+k\frac{1}{r}\frac{\partial T}{\partial \phi}\end{pmatrix},\quad \mathbf{G}_c=\begin{pmatrix}\varrho v_r\\ \varrho v_r v_x\\ \varrho v_r v_\phi\\ \varrho v_r^2+p\\ \varrho h_0 v_r\end{pmatrix},\quad \mathbf{G}_v=\begin{pmatrix}0\\ \tau_{rx}\\ \tau_{r\phi}\\ \tau_{rr}\\ \tau_{ri}v_i+k\frac{\partial T}{\partial r}\end{pmatrix},$$

$$\mathbf{H}_c=\frac{1}{r}\begin{pmatrix}0\\ 0\\ -\varrho v_r(v_\phi+2\Omega r)\\ \varrho(v_r+\Omega r)^2+p\\ 0\end{pmatrix},\quad \mathbf{H}_v=\frac{1}{r}\begin{pmatrix}0\\ 0\\ -\tau_{r\phi}\\ \tau_{\phi\phi}\\ 0\end{pmatrix}$$

which are formulated in a cylindrical coordinate system that rotates with an angular velocity Ω. Here v_x, v_ϕ and v_r represent the components of the relative velocity vector $\mathbf{v}=v_i$ in the x, ϕ and r directions and ϱ, p, T, k, h_0 denote density, pressure, temperature, thermal conductivity and relative specific total enthalpy $h_0=e_0+p/\varrho=h+\frac{1}{2}[v_x^2+v_\phi^2+v_r^2-(\Omega r)^2]$, respectively.

The stress tensor τ is calculated assuming a Newtonian fluid and the validity of the Stokesian hypothesis [22]. The temperature dependency of the viscosity is taken into account using Sutherland's law and the thermal conductivity is calculated assuming a constant Prandtl number. Turbulence effects are modeled using the Baldwin-Lomax [23] turbulence model. Finally, the general thermal and caloric equation of state $\varrho = \varrho(p,T)$ and $h = h(p,T)$ defined by the user close the Navier-Stokes equations.

3. Preconditioning

The derivation of the preconditioning matrix begins by transforming the independent variables in Equation (1) from the vector of conservative variables $\mathbf{Q}$ to the vector of viscous, primitive variables $\mathbf{Q}_v = (p, v_x, v_\phi, v_r, T)^T$ as follows:

$$\frac{\partial \mathbf{Q}}{\partial \mathbf{Q}_v}\frac{\partial \mathbf{Q}_v}{\partial t} + \frac{\partial(\mathbf{E}_c - \mathbf{E}_v)}{\partial x} + \frac{1}{r}\frac{\partial(\mathbf{F}_c - \mathbf{F}_v)}{\partial \phi} + \frac{1}{r}\frac{\partial[r(\mathbf{G}_c - \mathbf{G}_v)]}{\partial r} = \mathbf{H}_c - \mathbf{H}_v, \tag{2}$$

where the Jacobian $\frac{\partial \mathbf{Q}}{\partial \mathbf{Q}_v}$ is given by

$$\frac{\partial \mathbf{Q}}{\partial \mathbf{Q}_v} = \begin{pmatrix} \varrho_p & 0 & 0 & 0 & \varrho_T \\ v_x\varrho_p & \varrho & 0 & 0 & v_x\varrho_T \\ v_\phi\varrho_p & 0 & \varrho & 0 & v_\phi\varrho_T \\ v_r\varrho_p & 0 & 0 & \varrho & v_r\varrho_T \\ h_0\varrho_p - (1-\varrho h_p) & \varrho v_x & \varrho v_\phi & \varrho v_r & h_0\varrho_T + \varrho h_T \end{pmatrix}. \tag{3}$$

The indices p und T represent the isothermal derivative with respect to the pressure and the isobaric derivative with respect to the temperature, respectively; *i.e.* h_T is the specific isobaric heat capacity at constant pressure.

To ensure uniform, efficient convergence over all Mach numbers, the physical Jacobian is replaced with the preconditioning matrix Γ_v, so that the following equations

$$\Gamma_v\frac{\partial \mathbf{Q}_v}{\partial t} + \frac{\partial \mathbf{E}}{\partial x} + \frac{1}{r}\frac{\partial \mathbf{F}}{\partial \phi} + \frac{1}{r}\frac{\partial(r\mathbf{G})}{\partial r} = \mathbf{H} \tag{4}$$

with $\mathbf{E} = \mathbf{E}_c - \mathbf{E}_v$, $\mathbf{F} = \mathbf{F}_c - \mathbf{F}_v$, $\mathbf{G} = \mathbf{G}_c - \mathbf{G}_v$ and $\mathbf{H} = \mathbf{H}_c - \mathbf{H}_v$ have to be solved. As first proposed by Merkle *et al.* [19], the generality of the state equations of the fluid is retained when Γ_v is chosen in a form analogous to the Jacobian $\frac{\partial \mathbf{Q}}{\partial \mathbf{Q}_v}$:

$$\Gamma_v = \begin{pmatrix} \varrho'_p & 0 & 0 & 0 & \varrho'_T \\ v_x\varrho'_p & \varrho & 0 & 0 & v_x\varrho'_T \\ v_\phi\varrho'_p & 0 & \varrho & 0 & v_\phi\varrho'_T \\ v_r\varrho'_p & 0 & 0 & \varrho & v_r\varrho'_T \\ h_0\varrho'_p - h'_p & \varrho v_x & \varrho v_\phi & \varrho v_r & h_0\varrho'_T + \varrho h'_T \end{pmatrix}. \tag{5}$$

The preconditioning matrix differs only by the change of the partial derivatives ϱ_p, ϱ_T, h_T and $1-\varrho h_p$ that represents the physical properties by the artificial property terms ϱ'_p, ϱ'_T, h'_T, and h'_p, respectively. In the following sections, it will be shown how these quantities can be chosen to ensure well-conditioned flow equations at all Mach and Reynolds numbers.

3.1. Eigenvalue control for convergence acceleration

Assuming $h'_T = h_T$ and $h'_p = h_p$ the eigenvalues of the linearized unsteady Euler-equations in the ξ-direction on a grid-conformal, curvilinear $\xi-\eta-\zeta$ coordinate system are according to [24] given by

$$\lambda_{\xi_{1,2,3}} = \hat{U}, \quad \lambda_{\xi_{4,5}} = \frac{1}{2}\hat{U}\left(1+\frac{d}{d'}\right) \pm \frac{1}{2}\sqrt{\hat{U}^2\left(1-\frac{d}{d'}\right)^2 + 4\frac{\varrho h_T}{d'}\left(\xi_x^2+\xi_y^2+\xi_z^2\right)} \tag{6}$$

with

$$d = \varrho h_T \varrho_p + \varrho_T(1-\varrho h_p) \quad \text{and} \quad d' = \varrho h_T \varrho'_p + \varrho'_T(1-\varrho h_p). \tag{7}$$

The term $\hat{U} = u\xi_x + v\xi_y + w\xi_z$ represents the velocity component along the grid direction ξ with u, v and w representing the Cartesian velocity components. When preconditioning is not used, $d = d'$, and the last two eigenvalues should equal the propagation velocities of the pressure waves. Therefore the isentropic speed of sound is given by[1]

$$\left(\frac{\partial p}{\partial \varrho}\right)_s \equiv c^2 = \frac{\varrho h_T}{\varrho_T(1-\varrho h_p) + \varrho \varrho_p h_T}. \tag{8}$$

Consequently, the ratio $\varrho h_T/d'$ may be interpreted as an artificial speed of sound squared, c'^2. In order to avoid eigenvalue stiffness caused by the disparity of acoustic and convective velocities for subsonic flows, this artificial speed of sound is reduced to the particle velocity according to

$$c' = \sqrt{\frac{\varrho h_T}{d'}} := V_p, \quad \text{with} \quad V_p = \min(\mathbf{v}, c). \tag{9}$$

Combining Equations (7) and (9) results in the following prescription for the preconditioning parameter ϱ'_p:

$$\varrho'_p = \frac{1}{V_p^2} - \frac{\varrho'_T(1-\varrho h_p)}{\varrho h_T}. \tag{10}$$

The particle velocity is limited by the sonic speed, so if the other preconditioning parameters are set to their corresponding physical values, at supersonic speed the scaled flow Equations (4) and the physical Navier-Stokes equations (1) become identical. Preconditioning is not necessary at supersonic speed, since the original scheme is efficient for supersonic flows and eigenvalue stiffness first occurs at hypersonic speeds. The prescription for the preconditioning parameter ϱ'_p given by Equation (10) can also be derived using perturbation analysis for low Mach numbers and requiring that the temporal pressure derivative has to be retained in the continuity equation [15, 26].

In the incompressible limit the energy equation is decoupled from the continuity and momentum equations. This property is also desirable for the preconditioned equations, wherefore the preconditioning parameter ϱ'_T should be scaled proportional

1. A direct derivation of this relation by means of basic thermodynamic relations can be found in [25].

to its physical counterpart ϱ_T. In the solution scheme presented here ϱ'_T is set according to

$$\varrho'_T = \delta \cdot \varrho_T, \tag{11}$$

where the parameter δ is defined by the user.[2] With this choice of preconditioning parameters, by combining Equations (6), (8), (9), it can easily be shown that the condition number σ tends to $\sigma = \frac{|1+\sqrt{5}|}{|1-\sqrt{5}|} \approx 2.61$ for $\mathbf{v} \to 0$.

For an incompressible fluid with $\varrho = \text{const.}$ the sonic speed is infinite and the time derivatives in the continuity equation vanishes. By using preconditioning and setting $c' = V_p = \mathbf{v}$ for this case, time derivatives of pressure are added to the physical continuity equation. For the special case of $V_p = \sqrt{2} \cdot \mathbf{v}$ the preconditioning technique results in the artificial compressibility approach of Chorin [2]. This choice leads to the optimal condition number of $\sigma = 2$, valid for all speeds. The physical values $\varrho_T = \varrho_p = 0$ that cause the sonic velocity in incompressible fluids to be infinite are replaced with the artificial properties ϱ'_p and ϱ'_T. Done properly, this replacement alleviates the decoupling between the pressure and momentum terms in incompressible flows, and makes time-marching practical for both incompressible and low speed compressible flow computations.

3.2. Robustness considerations

In order to prevent singularities at solid walls, not v but the maximum of v and $V_{\text{lim}} = \epsilon_{\text{lim}} \cdot c$ is used as the particle velocity for subsonic flows, where ϵ_{lim} typically is set to 10^{-5}. As will be shown in Chapter 6, preconditioning yields a significant enhancement of the convergence rates at low Mach numbers. However, as discussed in [27], preconditioned systems show an increased sensitivity to pressure fluctuations and are unstable in the presence of pressure fluctuations that are large compared to the dynamic pressure, ϱu^2, especially in the initial phase of a simulation. One approach devised by Weiss *et al.* [28] to handle this sensitivity to pressure fluctuations is to introduce the term $V_{\text{pgr}} = \epsilon_{\text{pgr}} \sqrt{\frac{\delta p}{\varrho}}$ and limit the pseudo-acoustic speed c' for the case of a compressible fluid according to

$$c' = V_p = \min[c, \max(\mathbf{v}, V_{\text{lim}}, V_{\text{pgr}})]. \tag{12}$$

In the presented work this modification was adopted with the pressure variation δp taken as the maximum pressure variation within a control volume and $\epsilon_{\text{pgr}} \in [0.1, 1.0]$.

3.3. Scaled equations for low Reynolds number flow

The preconditioned scheme presented so far is capable of calculating inviscid flows efficiently at arbitrary Mach numbers. However, as recognized by Choi and Merkle [10] additional modifications are necessary in order to retain an efficient scheme for viscous flows. Even though flows in turbomachinery applications usually have high Reynolds numbers where it could be anticipated that the dominant characteristics controlling the solution of the Navier-Stokes equations are the same as those of the Euler equations, the Reynolds numbers of the cross stream directions in the boundary

2. As shown in [24], for the choice $\delta = 0$ the preconditioning matrix is regular for every physical state and positive values of ϱ'_p. In order to retain regularity of the preconditioning matrix for the special case of a perfect gas, the parameter δ should not exceed unity.

layers are small. In the following the necessary modifications for also calculating the diffusion-dominated flow efficiently will be described.

Using the perturbation analysis in the low Reynolds number case, Venkateswaran and Merkle [27] show that the preconditioning parameter ϱ'_T should scale according to

$$\varrho'_T \propto \varrho_T \mathrm{Re}/T_r \tag{13}$$

in order to prevent the temporal derivative of the temperature from appearing in the momentum equation. T_r is a reference temperature and Re is an appropriate Reynolds number. In the present work this preconditioning parameter was not scaled with the Reynolds number and the inviscid prescription, Equation (11), was also used for the viscous case. Even though the viscous restriction given by Equation (13) can be satisfied setting $\delta := 0$, varying this parameter from $\delta = 1$ to $\delta = 0$ did not prove to have any effect on the presented results.[3]

According to [26], scaling of the energy equation setting $h'_T = h_T/\mathrm{Pr}$ is appropriate if the Prandtl number is deviating largely from unity. Since most fluids have Prandtl numbers near unity, this modification was not adopted in our scheme.

The temporal term in the continuity equation balances the convective term at low Reynolds numbers, provided that $\varrho'_p \propto \mathrm{Re}^2/V_p^2$ holds, where Re is an appropriate Reynolds number [26]. Using a Fourier stability analysis [27], it can be shown that the proper Reynolds number scale is to use the cell-Reynolds number, $\mathrm{Re}_{\Delta x} = u\Delta x/\nu$. This limit can be incorporated in the following manner for the compressible case: the particle velocity V_p from which the preconditioning parameter ϱ'_p is determined is calculated according to

$$V_p = \min(c, \max(\mathbf{v}, V_{\mathrm{lim}}, V_{\mathrm{pgr}}, V_{\mathrm{vis}})), \tag{14}$$

where V_{vis} is given by $V_{\mathrm{vis}} = \frac{\nu}{\Delta x}$ which represents the velocity scale of diffusion of momentum. The introduction of the cell-Reynolds number shows that whether low Mach preconditioning or low Reynolds preconditioning is used, depends on both the flow field and the grid resolution. An examination of Equation (14) shows that the introduction of the diffusion velocity scale V_{vis} may reduce the inviscid preconditioning. When active, the low Reynolds number scaling causes the convective terms to be stiff, but since in this case the viscous terms dominate, the convective fluxes are neglectable and do not inhibit the convergence.

4. Solution procedure

4.1. Spatial discretization

The preconditioned governing Equations (4) are cast in integral, cylindrical form for an arbitrary control volume V with surface A as follows:

$$\Gamma_v \int_V \frac{\partial \mathbf{Q}_v}{\partial t} dV + \int_A (\mathbf{E} r d\phi dr + \mathbf{F} dx d\phi + \mathbf{G} r dx d\phi) + \int_V \mathbf{H} dV = 0. \tag{15}$$

3. Using $\delta = 1$ gives a more complicated preconditioning matrix than for the case of $\delta = 0$. However, the former choice eases the calculation of eigenvectors.

These equations are discretized centrally in space using a finite-volume scheme wherein the physical domain is subdivided into curved hexahedral control volumes $\hat{V}_{i,j,k}$. The spatial discretization of the integral equations is written as

$$\Gamma_v \frac{\partial \mathbf{Q}_{v_{i,j,k}}}{\partial t} = -\frac{1}{V_{i,j,k}}(\mathbf{R}_C + \mathbf{R}_D + \mathbf{D}), \tag{16}$$

where $\mathbf{R}_C$ and $\mathbf{R}_D$ is the sum of convective and diffusive fluxes and sources, respectively, while $\mathbf{D}$ represents the artificial dissipation. The values of the solution vector are located at the vertices of the cells. In ITSM3D the discretization scheme developed by Radespiel and Rossow [29] was adopted, where the control volume for calculating the convective fluxes associated with the grid point (i,j,k) consists of the eight surrounding cells. The contribution of the viscous fluxes to the total residual are calculated using the corresponding dual mesh, *cf.* [22] for details.

To prevent odd-even point decoupling and eliminate high-wavenumber modes in the solution, artificial dissipation is added to the residual using an extension of the model introduced by Jameson *et al.* [5]. In order to have a scheme that is low diffusive where the flow field is smooth and is also capable of resolving shocks sharply, the artificial dissipation consists of a blend of second and fourth order differences of the solution variables along the grid directions ξ,η,ζ. The artificial dissipation associated with the control volume $\hat{V}_{i,j,k}$ is calculated as follows:

$$\mathbf{D}_{i,j,k} = \left(-D_\xi^2 + D_\xi^4 - D_\eta^2 + D_\eta^4 - D_\zeta^2 + D_\zeta^4\right)\mathbf{Q}_{v_{i,j,k}}, \tag{17}$$

with the second and fourth order difference operators which for the ξ-direction are given by

$$D_\xi^{(2)} = \delta_\xi^- \left(\bar{\rho}_\xi^V \varepsilon^{(2)} \Gamma_v\right)_{i+1/2,j,k} \delta_\xi^+, \qquad D_\xi^{(4)} = \delta_\xi^- \left(\bar{\rho}_\xi^V \varepsilon^{(4)} \Gamma_v\right)_{i+1/2,j,k} \delta_\xi^+ \delta_\xi^- \delta_\xi^+ \tag{18}$$

where δ_ξ^+ and δ_ξ^- denote the backward and forward difference operators, respectively. This formulation of the dissipation terms is conservative, and with this scheme one still can calculate transonic flows and resolve shocks sharply. However, there is a price to pay: The calculation of dissipation terms now involves the evaluation of a matrix-vector product; as a result, the numerical effort is equivalent in complexity to a matrix dissipation scheme. When conservativity can be sacrificed, which is of little concern for strictly subsonic flow, the dissipation terms in ITSM3D can be calculated according to

$$D_\xi^{(2)} = \delta_\xi^- \left(\bar{\rho}_\xi^V \varepsilon^{(2)}\right)_{i+1/2,j,k} \delta_\xi^+, \qquad D_\xi^{(4)} = \delta_\xi^- \left(\bar{\rho}_\xi^V \varepsilon^{(4)}\right)_{i+1/2,j,k} \delta_\xi^+ \delta_\xi^- \delta_\xi^+ \tag{19}$$

when specified by the user. Consistently, the dissipation terms are first added after the residuals are multiplied with the inverse preconditioning matrix but before integration is performed.

The scaling factor $\bar{\rho}_\xi^V$ could be calculated by simply adding the volume weighted spectral radii[4] for each grid direction, $\bar{\rho}_\xi^V = \rho_\xi^V + \rho_\eta^V + \rho_\zeta^V$. In order to minimize the artificial dissipation in the boundary layer the factors are calculated to

4. The unweighted spectral radius ρ_ξ for the ξ-direction is given by the fifth solution of Equation (6).

$$\bar{\rho}^V_{\xi_{i+1/2,j,k}} = \rho^V_{\xi_{i+1/2,j,k}} \left\{ 1 + \max \left[\left(\frac{\rho^V_{\eta_{i+1/2,j,k}}}{\rho^V_{\xi_{i+1/2,j,k}}} \right)^{1/2}, \left(\frac{\rho^V_{\zeta_{i+1/2,j,k}}}{\rho^V_{\xi_{i+1/2,j,k}}} \right)^{1/2} \right] \right\} \tag{20}$$

as proposed by Martinelli [30] and Radespiel *et al.* [31]. The coefficients $\varepsilon^{(2)}$ and $\varepsilon^{(4)}$ are determined from

$$\begin{aligned} \varepsilon^{(2)}_{i+1/2,j,k} &= k^{(2)} \max(\nu_{\xi_{i-1,j,k}}, \nu_{\xi_{i,j,k}}, \nu_{\xi_{i+1,j,k}}, \nu_{\xi_{i+2,j,k}}), \\ \varepsilon^{(4)} &= \max(0, k^{(4)} - \varepsilon^{(2)}_{i+1/2,j,k}). \end{aligned} \tag{21}$$

and depend on the pressure gradient of the solution

$$\nu_{\xi_{i,j,k}} = \left| \frac{p_{i-1,j,k} - 2p_{i,j,k} + p_{i+1,j,k}}{p_{i-1,j,k} + 2p_{i,j,k} + p_{i+1,j,k}} \right|. \tag{22}$$

The operators for the artificial dissipation in the η and ζ directions are defined analogously.

The spectral radii of the preconditioned system rather than spectral radii of the physical Euler equations are used for scaling the dissipation terms. As demonstrated by [27, 32], using the spectral radius of the Euler equations the dissipation terms would not scale properly in the low Mach number limit. The added dissipation to the continuity equation would become disappearingly small; as shown in [33], under such conditions the pressure field shows odd-even splitting errors in the solution. At the same time the momentum and energy equations would suffer under excessive dissipation added. Also in the low Reynolds number limit the dissipation terms are only well-proportioned when the eigenvalues of the preconditioned system are used and the governing equations are preconditioned properly.

4.2. Time-stepping scheme

The system of ordinary differential equations (16) is discretized and advanced in time by an explicit five-stage time-stepping scheme introduced by Radespiel and Swanson [34]. It is given by

$$\begin{aligned} &\mathbf{Q}^{(0)}_{v_{i,j,k}} = \mathbf{Q}^{(n)}_{v_{i,j,k}}, \\ &\mathbf{Q}^{(s)}_{v_{i,j,k}} = \mathbf{Q}^{(0)}_{v_{i,j,k}} - \alpha_s \frac{\Delta t}{\hat{V}_{i,j,k}} \Gamma_v^{-1} \left(\mathbf{R}_C^{(s-1)} + \mathbf{R}_D^{(0)} + \sum_{t=1}^{s} \gamma_{st} \mathbf{D}^{(s-1)} \right)_{i,j,k} \qquad s = 1,2,\ldots,5 \\ &\mathbf{Q}^{(n+1)}_{v_{i,j,k}} = \mathbf{Q}^{(5)}_{v_{i,j,k}} \end{aligned} \tag{23}$$

with $\mathbf{R}_C^{(s-1)} = \mathbf{R}_C(\mathbf{Q}_v^{(s-1)})$, $\mathbf{R}_D^{(0)} = \mathbf{R}_D(\mathbf{Q}_v^{(0)})$, $\mathbf{D}^{(s-1)} = \mathbf{D}(\mathbf{Q}_v^{(s-1)})$ and the coefficients

$$\begin{gathered} \gamma_{11} = \gamma_{21} = 1, \quad \gamma_{22} = 0, \quad \gamma_{31} = \gamma_{41} = \frac{11}{25}, \quad \gamma_{32} = \gamma_{42} = 0, \quad \gamma_{33} = \gamma_{43} = \frac{14}{25}, \quad \gamma_{44} = 0, \\ \gamma_{51} = \frac{154}{625}, \quad \gamma_{52} = 0, \quad \gamma_{53} = \frac{196}{625}, \quad \gamma_{54} = 0, \quad \gamma_{55} = \frac{11}{25}, \\ \alpha_1 = \frac{1}{4}, \quad \alpha_2 = \frac{1}{6}, \quad \alpha_3 = \frac{3}{8}, \quad \alpha_4 = \frac{1}{2}, \quad \alpha_5 = 1. \end{gathered} \tag{24}$$

The scheme is hybrid since the artificial dissipation and the diffusive terms are not calculated at every stage, which increases the computational efficiency by an unaltered

maximum CFL number of $\mathrm{CFL}_{\max} = 4$ and simultaneously raises the maximum stable von Neumann number from $\mathrm{VNN}_{\max} = 2.59$ to $\mathrm{VNN}_{\max} = 9$.

As derived in [22], the maximum stable time step of the non-preconditioned solution scheme for the Navier-Stokes equations is given by

$$\Delta t_{\max} = \frac{\mathrm{CFL}_{\max}}{\rho_\xi + \rho_\eta + \rho_\zeta + 4 \cdot \max(4/3\nu, \alpha) \cdot \frac{\mathrm{CFL}_{\max}}{\mathrm{VNN}_{\max}} (\nabla\xi^2 + \nabla\eta^2 + \nabla\zeta^2)}, \tag{25}$$

where α represents the effective thermal diffusitivity. In the derivation of this relation only assumptions were made regarding the solution scheme and the diffusive transport processes. This is reflected by the fact that the quantities $\mathrm{CFL}_{\max}$ and $\mathrm{VNN}_{\max}$ in Equation (25) are only dependent on the solution scheme and not on the equations solved. These quantities limit the maximum stable propagation per time step of the convective and diffusive processes the solution scheme can admit before solution decoupling and instability occurs. Further, the circumstance that the convection processes are only represented by the eigenvalues clearly show that the relation (25) holds for arbitrary convective processes. The preconditioned scheme presented here alters only the convective velocities[5] and leaves the diffusion rates to their physical values.[6] Consequently, the time step limitation given by Equation (25) also holds for the preconditioned scheme used when ρ_ξ, ρ_η and ρ_ζ represent the unweighted spectral radii of the preconditioned system and not the unweighted spectral radii of the linearized Euler equations.

4.3. Boundary treatment

For the steady state numerical simulation of turbine flows, six different types of boundaries have to be considered: Inlet, outlet, non-rotating and rotating walls, periodicity and mixing planes.

Solid walls are assumed to be adiabatic, and the no-slip condition is applied. Periodicity in the pitch-wise direction is ensured using phantom cells that keep copies of the periodic values such that the points on these boundaries can be treated like interior points.

At the inlet and outlet boundaries and at the mixing planes a non-reflecting post-correction method is used. The boundary conditions used represents an extension of the work of Giles [20] and Saxer [35] to preconditioned systems with arbitrary equations of state and the essential elements of the developed theory will be presented in the following chapter.

5. Non-reflecting boundary conditions for preconditioned systems

In the original scheme of the flow solver ITSM3D the non-reflecting boundary treatment developed by Giles [20] and Saxer [35] is used. In the approach adopted, the solution at the boundary is decomposed into Fourier modes, where the zeroth

5. If $h'_T = h_T$ and $h'_p = h_p$ preconditioning only changes the acoustic velocities, which easily can be seen from Equation (6).

6. In the low Reynolds number limit, preconditioning equalizes the acoustic and diffusive velocities only by scaling the acoustic velocities not the diffusive velocities.

mode corresponds to the average solution. This average mode is treated according to standard one-dimensional characteristic theory and enables the user to specify the circumferential averages of certain flow field parameters at the boundary. The remaining harmonics of the solution at the boundary are altered to satisfy a condition derived by Giles [20] basing on the linearized, two-dimensional Euler-equations, which ensures that the variations corresponding to incoming waves are eliminated. Using the quasi-three-dimensional approach of Saxer [35], the grid layers in the radial direction are treated independently, wherefore the needed Fourier decomposition of the state variables at the boundary is limited to the circumferential direction. This method is motivated by the fact that in axial turbomachinery the flow field variations are usually larger in pitchwise direction than in the radial direction.

The use of the quasi-three-dimensional non-reflecting boundary conditions in the combination with the original scheme has proven to be successful; applying these boundary conditions, several multi-stage, high-speed turbomachinery applications with small spacing between the blade rows have been simulated accurately [22, 36].

The preconditioned scheme described in the previous chapters was first used with the original, non-reflecting boundary treatment, thereby frequently encountering instabilities in the vicinity of the boundaries. In Chapter 6 it will be demonstrated that at low Mach numbers the use of unmodified boundary conditions in conjunction with preconditioning can indeed lead to instability of the integration scheme and deterioration of accuracy. As already stated in the Introduction, from a theoretical point of view it is obvious that a change of the dynamics of the equations solved due to preconditioning makes it necessary to modify the original boundary conditions. Thus, a derivation of the appropriate boundary conditions for the presented preconditioning method for arbitrary equations of state was performed and in this chapter the necessary framework for a successful implementation will be presented.

In the following section the Giles-condition for a non-reflecting boundary for the preconditioned system will be established. After reviewing the quasi-three-dimensional approach due to Saxer in Chapter 5.2, the one-dimensional characteristic boundary conditions for preconditioned systems will be presented in Chapter 5.3. With the one-dimensional boundary treatment as a basis, in Chapter 5.4 the completing theory for a non-reflecting correction of the spatial harmonics will be given.

5.1. The Giles-condition for a non-reflecting boundary

In order to arrive at the Giles-condition for a non-reflecting boundary, we start our analysis linearizing the preconditioned Navier-Stokes equations (4) about the average state vector $\bar{\mathbf{Q}}_v$. Neglecting the diffusive fluxes and the source terms, the following equations are obtained

$$\Gamma_v \frac{\partial \tilde{\mathbf{Q}}_v}{\partial t} + A\frac{\partial \tilde{\mathbf{Q}}_v}{\partial x} + B\frac{\partial \tilde{\mathbf{Q}}_v}{\partial y} + C\frac{\partial \tilde{\mathbf{Q}}_v}{\partial z} = 0 \tag{26}$$

for the perturbed state variable $\tilde{\mathbf{Q}}_v = \mathbf{Q}_v - \bar{\mathbf{Q}}_v$ with the matrices A, B, C given by $A = \frac{\partial \mathbf{E}_c}{\partial \mathbf{Q}_v}|_{\bar{\mathbf{Q}}_v}$, $B = \frac{\partial \mathbf{F}_c}{\partial \mathbf{Q}_v}|_{\bar{\mathbf{Q}}_v}$, $C = \frac{\partial \mathbf{G}_c}{\partial \mathbf{Q}_v}|_{\bar{\mathbf{Q}}_v}$. To simplify the analysis Cartesian coordinates are now used; substituting (v_x, v_ϕ, v_r) with (u, v, w) the convective terms in Equation (1) can otherwise be kept unchanged. In order to separate waves into

incoming and outgoing waves, the perturbed state variable is decomposed into Fourier modes

$$\tilde{\mathbf{Q}}_v(x,y,z,t) = \sum_{l=-\infty}^{\infty} \hat{\mathbf{q}}_l^R e^{\hat{\imath}(-\omega_l t + x k_{x_l} + y k_{y_l} + z k_{z_l})}. \tag{27}$$

Applying this decomposition to the linearized Euler equations leads to the following relation

$$\begin{aligned} 0 &= (-\omega\Gamma_v + k_x A + k_y B + k_z C)\hat{\mathbf{q}}^R \\ &= \underbrace{(-\omega I + k_x\Gamma_v^{-1}A + k_y\Gamma_v^{-1}B + k_z\Gamma_v^{-1}C)}_{A_q}\hat{\mathbf{q}}^R \end{aligned} \tag{28}$$

for any mode with the wave number k_x, k_y, k_z, frequency ω, and amplitude $\hat{\mathbf{q}}^R$. Nontrivial solutions $\hat{\mathbf{q}}^R$ of Equation (28) only exist when the dispersion relation $|A_q| = 0$ holds; it relates the wave numbers k_x, k_y, k_z to the frequency ω over a homogeneous fifth-order polynomial expression. As can be seen from Equation (28), $\hat{\mathbf{q}}^R$ is a right eigenvector of the matrix $\check{A}_\Gamma$ given by

$$\check{A}_\Gamma = \Gamma_v^{-1}(k_x A + k_y B + k_z C). \tag{29}$$

A key point in the construction of a non-reflecting boundary is to use orthogonality relations to discard spatial variations of the state variables representing incoming waves. When the eigenvalues $\omega_i; i = 1,2,\ldots,5$ of the matrix $\check{A}_\Gamma \in \mathbb{R}^{5\times 5}$ are distinct, the following orthogonality relation between the left eigenvector $\hat{\mathbf{q}}_n^L$ and the right eigenvector $\hat{\mathbf{q}}_n^R$ holds

$$(\hat{\mathbf{q}}_n^L)^T(\omega_n,k_x,k_y,k_z)\cdot\hat{\mathbf{q}}_m^R(\omega_m,k_x,k_y,k_z) = 0, \quad \forall\omega_n \neq \omega_m, \tag{30}$$

which can also be expressed as

$$L\cdot R = I, \quad \text{with} \quad L = (\hat{\mathbf{q}}_1^L,\ldots,\hat{\mathbf{q}}_5^L)^T, R = (\hat{\mathbf{q}}_1^R,\ldots,\hat{\mathbf{q}}_5^R). \tag{31}$$

Even if there are identical eigenvalues, the eigenvectors $\hat{\mathbf{q}}_n^L$ and $\hat{\mathbf{q}}_n^R$ can still be constructed to achieve orthogonality according to Equation (31), provided the multiplicity r of the eigenvalue ω_i equals the rank deficiency of the matrix $\check{A}_\Gamma - \omega_i I$, or expressed mathematically, $\mathrm{Ran}(\check{A}_\Gamma - \omega_i I) = \mathrm{Ran}(\check{A}_\Gamma) - r$. This is in fact the case for the preconditioned Euler equations, which is proved by the existence of L and R given by Equation (74).

The left and right eigenvectors $\hat{\mathbf{q}}_i^L$ and $\hat{\mathbf{q}}_i^R$ are orthogonal to each other for different frequencies ω but the same wave numbers k_x, k_y, k_z. However, as will become clear in the following, in order to arrive at a non-reflecting condition, we need a set of vectors $\hat{\mathbf{p}}_i^T$ that are orthogonal to the right eigenvectors $\hat{\mathbf{q}}_i^L$ for different wave numbers k_{x_i} and the same values of ω, k_y, k_z satisfying the dispersion relation $|A_q| = 0$. We therefore introduce $\hat{\mathbf{p}}_i^L$ as a left eigenvector of the matrix $-\omega A^{-1}\Gamma_v + k_y A^{-1}B + k_z A^{-1}C$ with the eigenvalue $-k_{x_i}$, *i.e.*

$$\begin{aligned} \mathbf{0} &= (\hat{\mathbf{p}}_i^L)^T A^{-1}\Gamma_v \underbrace{(-\omega I + k_x\Gamma_v^{-1}A + k_y\Gamma_v^{-1}B + k_z\Gamma_v^{-1}C)}_{A_q} \\ &= (\hat{\mathbf{p}}_i^L)^T \underbrace{(-\omega A^{-1}\Gamma_v + k_x I + k_y A^{-1}B + k_z A^{-1}C)}_{A_p}, \quad \forall i = 1,2,\ldots,5 \end{aligned} \tag{32}$$

with the desired property

$$(\hat{\mathbf{p}}_n^L)^T(\omega,k_{x_n},k_y,k_z)\cdot\hat{\mathbf{q}}_m^R(\omega,k_{x_m},k_y,k_z)=0,\qquad \forall k_{x_n}\neq k_{x_m}. \tag{33}$$

The validity of this orthogonality relation (33) can be verified by multiplying the equation $A_p\hat{\mathbf{q}}_n^R=\mathbf{0}$ from the left with $(\hat{\mathbf{p}}_m^L)^T$ and the equation $(\hat{\mathbf{p}}_m^L)^TA_p=\mathbf{0}$ from the right with $\hat{\mathbf{q}}_n^R$ and subtracting the last equation from the first.

Suppose the differential equations are to be solved on a domain $x\in[0,1]$ and one wants to eliminate reflections at the boundary $x=0$. For one particular choice of ω, k_y, k_z the perturbed state vector $\tilde{\mathbf{Q}}_v$ can be decomposed according to

$$\tilde{\mathbf{Q}}_v=\left(\sum_{n=1}^{5}a_n\hat{\mathbf{q}}_n^Re^{\hat{\imath}k_{x_n}x}\right)e^{\hat{\imath}(k_yy+k_zz-\omega t)}, \tag{34}$$

with k_{x_n} representing a root of the dispersion relation. Reflections at the boundary can now be prevented by specifying $a_n=0$ for each n corresponding to an incoming wave. An equivalent condition for a non-reflecting boundary is

$$(\hat{\mathbf{p}}_n^L)^T\cdot\tilde{\mathbf{Q}}_v:=0, \tag{35}$$

for all left special eigenvectors $\hat{\mathbf{p}}_n^L$ belonging to a mode traveling towards the boundary. Using the orthogonality relation given by Equation (33), the last condition follows immediately from

$$\begin{aligned}(\hat{\mathbf{p}}_n^L)^T\cdot\tilde{\mathbf{Q}}_v=&(\hat{\mathbf{p}}_n^L)^T\left[\sum_{m=1}^{5}a_m\hat{\mathbf{q}}_m^Re^{\hat{\imath}xk_{x_m}}\right]e^{\hat{\imath}(-\omega t+yk_y+zk_z)}\\ =&a_n\left[(\hat{\mathbf{p}}_n^L)^T\hat{\mathbf{q}}_n^R\right]e^{\hat{\imath}xk_{x_n}}e^{\hat{\imath}(-\omega t+yk_y+zk_z)}\\ :=&0.\end{aligned} \tag{36}$$

5.2. The Giles-Saxer quasi-3D steady non-reflecting boundary conditions

In the last section the Giles-condition for a non-reflecting boundary was reviewed for the general three-dimensional, unsteady case and the necessary left eigenvectors were defined for the case of preconditioning. As mentioned earlier, assuming that the variations in the spanwise directions are small compared to the variations in the circumferential directions, the needed Fourier transform for implementing the Giles-condition given by Equation (35) can be limited to the circumferential direction by setting $k_z:=0$. Since this method considers radial flow variations in the average mode only, Saxer [35] named it quasi-three-dimensional. In this approach the curvature of the radial grid layers at the boundary is neglected and the boundary conditions for an annular cascade are obtained simply by substituting (ϕ,r) for (y,z), and (v_ϕ,v_r) for (v,w) when applying the Giles-condition given by Equation (35).

Since steady flows are considered, we are only interested in boundary conditions in the limit of a converged solution with $\omega\to0$. At the boundary $x=x_0$ with $k_z:=0$

and $\omega \to 0$ the wave representation of the perturbed state variable according to Equation (27) can be simplified to

$$\tilde{\mathbf{Q}}_v(x_0,z) = \sum_{m=-\infty}^{\infty} \hat{\mathbf{q}}_m(x_0,z)\cdot e^{\hat{\imath} y k_{y_m}} = \bar{\mathbf{q}}(x_0,z) + \sum_{\substack{m=-\infty \\ m\neq 0}}^{\infty} \hat{\mathbf{q}}_m(x_0,z)\cdot e^{\hat{\imath} y k_{y_m}}. \tag{37}$$

$\bar{\mathbf{q}}(x,z)$ corresponds to the zeroth Fourier mode and represents the pitchwise solution average at the boundary specified using the one-dimensional characteristic boundary theory for preconditioned systems given in the next Chapter. At every spanwise location, the Giles-condition, Equation (35), is applied for every Fourier mode $m \neq 0$. In the limit of $k_y/\omega \to \infty$ and $k_z := 0$ the left special eigenvectors defined in Equation (32) can after a considerable amount of algebra be calculated to

$$\begin{aligned}
\begin{pmatrix} \hat{\mathbf{p}}_1^T \\ \cdots \\ \hat{\mathbf{p}}_5^T \end{pmatrix}_{\text{comp}} &= \begin{pmatrix} -\frac{1-\varrho h_p}{\varrho h_T} & 0 & 0 & 0 & 1 \\ -\frac{1}{\varrho} & -u & -v & 0 & 0 \\ 0 & 0 & 0 & 1 & 0 \\ -\beta & \varrho v c & -\varrho u c & 0 & 0 \\ \beta & \varrho v c & -\varrho u c & 0 & 0 \end{pmatrix}, \\
\begin{pmatrix} \hat{\mathbf{p}}_1^T \\ \cdots \\ \hat{\mathbf{p}}_5^T \end{pmatrix}_{\text{incomp}} &= \begin{pmatrix} -\frac{1-\varrho h_p}{\varrho h_T} & 0 & 0 & 0 & 1 \\ -\frac{1}{\varrho} & -u & -v & 0 & 0 \\ 0 & 0 & 0 & 1 & 0 \\ \gamma & -\varrho v & \varrho u & 0 & 0 \\ -\gamma & -\varrho v & \varrho u & 0 & 0 \end{pmatrix}.
\end{aligned} \tag{38}$$

$(\hat{\mathbf{p}}_1,\ldots,\hat{\mathbf{p}}_5)^T_{\text{comp}}$ represents the complete set of left special eigenvectors for the compressible case with the general thermal equation of state $\varrho = \varrho(p,T)(\varrho_p \neq 0)$ and $(\hat{\mathbf{p}}_1,\ldots,\hat{\mathbf{p}}_5)^T_{\text{incomp}}$ describes the corresponding eigenvectors for the case of an incompressible fluid with $\varrho = \text{const.}$ as the thermal state equation. The parameters β and γ are given by

$$\gamma = \hat{\imath}\cdot\text{sign}(k_y), \quad \beta = \begin{cases} \hat{\imath}\cdot\text{sign}(k_y)\sqrt{c^2-(u^2+v^2)}, & u^2+v^2 \leq c^2, \\ -\text{sign}(v)\sqrt{(u^2+v^2)-c^2}, & u^2+v^2 \geq c^2. \end{cases} \tag{39}$$

The first left special eigenvector for the compressible case presented here differs from the result obtained by Saxer [35] since we use a different set of primitive variables and a general and not an ideal representation of state. However, the four last eigenvectors correspond to the eigenvectors derived by Saxer, which can be explained by the fact that preconditioning does not affect the steady state. Because the physical speed of sound is infinite in incompressible fluids, it is obvious that the eigenvectors $(\hat{\mathbf{p}}_1,\ldots,\hat{\mathbf{p}}_5)^T_{\text{comp}}$ cannot be used for the incompressible case. The eigenvectors $(\hat{\mathbf{p}}_1,\ldots,\hat{\mathbf{p}}_5)^T_{\text{incomp}}$ were derived taking the property $\varrho = \text{const.}$ into account.

5.3. One-dimensional characteristic boundary conditions

5.3.1. Axially subsonic inlet

The average changes in the four incoming characteristics are calculated from the requirement that the average flow field match the total temperature $T_{0,bc}(r)$, the

total pressure $p_{0,bc}(r)$, the relative flow angle $\beta_{bc}(r)$ in the n-ϕ-plane and the pitch angle $\gamma_{bc}(r)$ in the n-t-plane specified by the user. Accordingly, in the following u, v, w represent the velocity component in the normal, circumferential and tangential direction of the boundary, respectively. An equivalent specification of the average inlet conditions is to drive to zero the following boundary residuals:

$$\begin{aligned} R_1 &:= \bar{\varrho}\bar{T}(\bar{s}-s_{bc}(r)), & R_2 &:= \bar{\varrho}\bar{c''}(\bar{v}-\bar{u}\tan\beta_{bc}(r)), \\ R_3 &:= \bar{\varrho}\bar{c''}(\bar{w}-\bar{u}\tan\gamma_{bc}(r)), & R_4 &:= \bar{\varrho}(\bar{h}_0-h_{0,bc}(r)) \end{aligned} \tag{40}$$

with the entropy and total enthalpy given by $s_{bc} = s(p_{0,bc},T_{0,bc})$ and $h_{0,bc} = h(p_{0,bc},T_{0,bc})$, respectively.[7] A bar " $\bar{}$ " denotes a circumferential average of the respective quantity. The nonlinear Equations (40) are linearized about the circumferentially averaged solution $\bar{\mathbf{Q}}_v^{(n)}$ of the last time-step n

$$\begin{aligned} \mathbf{R}^{(n+1)} &= \mathbf{R}^{(n)} + \underbrace{\frac{\partial(R_1,R_2,R_3,R_4)}{\partial(\phi_1,\phi_2,\phi_3,\phi_4)}}_{J}\Bigg|_{\bar{\mathbf{Q}}_v^{(n)}} \cdot \begin{pmatrix} \delta\bar{\phi}_1 \\ \delta\bar{\phi}_2 \\ \delta\bar{\phi}_3 \\ \delta\bar{\phi}_4 \end{pmatrix}^{(n)} := 0, \\ J &= \frac{\partial(R_1,R_2,R_3,R_4)}{\partial(p,u,v,w,T)} \underbrace{\frac{\partial(p,u,v,w,T)}{\partial(\phi_1,\phi_2,\phi_3,\phi_4)}}_{(\mathbf{r}_1,\mathbf{r}_2,\mathbf{r}_3,\mathbf{r}_4)} \end{aligned} \tag{41}$$

where $\mathbf{r}_i; i = 1,\ldots,4$ represent the first four right eigenvectors given by Equation (74). When solving these linearized equations one obtains the necessary variations of the average incoming characteristic variables $\delta\bar{\phi}_i^{(n)} = \bar{\phi}_i^{(n+1)} - \bar{\phi}_i^{(n)}; i = 1,\ldots,4$ for driving the boundary residuals with increasing time-step to zero.

As can be proven, the relation $\frac{1-\varrho h_p}{\varrho h_T} + \frac{s_p}{s_T} = 0$ holds for general equations of state wherefore the average variations of the characteristics can be calculated to

$$\begin{aligned} \begin{pmatrix} \delta\bar{\phi}_1 \\ \delta\bar{\phi}_2 \\ \delta\bar{\phi}_3 \\ \delta\bar{\phi}_4 \end{pmatrix}^{(n)} &= -J^{-1}\big|_{\bar{\mathbf{Q}}_v^{(n)}} \cdot \mathbf{R}^{(n)} = \\ &= -\begin{pmatrix} \frac{1}{\varrho h_T} & 0 & 0 & 0 \\ -\frac{\beta^*_{bc}}{\varrho c'' M''} & \frac{M''-M''_y\beta^*_{bc}}{\varrho c'' M''} & -\frac{M''_z\beta^*_{bc}}{\varrho c'' M''} & \frac{\beta^*_{bc}}{\varrho c'' M''} \\ -\frac{\gamma^*_{bc}}{\varrho c'' M''} & -\frac{M''_y\gamma^*_{bc}}{\varrho c'' M''} & \frac{M''-M''_z\gamma^*_{bc}}{\varrho c'' M''} & \frac{\gamma^*_{bc}}{\varrho c'' M''} \\ -\frac{2}{M''} & -\frac{2M''_y}{M''} & -\frac{2M''_z}{M''} & \frac{2}{M''} \end{pmatrix}_{\bar{\mathbf{Q}}_v^{(n)}} \cdot \begin{pmatrix} R_1 \\ R_2 \\ R_3 \\ R_4 \end{pmatrix}^{(n)} \end{aligned} \tag{42}$$

with the Mach numbers M'', M''_y, M''_z and the abbreviations Γ, β^*_{bc}, γ^*_{bc} given by

$$\begin{aligned} M'' &= \frac{\Gamma}{c''}, \quad M''_y = \frac{v}{c''}, \quad M''_z = \frac{w}{c''}, \\ \Gamma &= c'' + u'' + v\beta^*_{bc} + w\gamma^*_{bc}, \quad \beta^*_{bc} = \tan\beta_{bc}, \quad \gamma^*_{bc} = \tan\gamma_{bc}. \end{aligned} \tag{43}$$

7. For the definition of the first boundary residual Giles [20] uses the entropy related function s^* with $s^* := \ln(p) - \kappa\ln\varrho$, which for ideal gases corresponds to $s^* = \frac{s}{c_v}$. Since the specific isochore heat capacity neither can be calculated directly from $\varrho = \varrho(p,T)$, $h = h(p,T)$ nor from $s = s(p,T)$, and since specifying $s^* := \text{const.}$ does not necessarily enforce $s = \text{const.}$ for general equations of state, the entropy function is used directly.

The quantities c'', u_0'' and u'' are defined according to Equation (75) given in Appendix 8.1. The determinant D of the Jacobian J is given by

$$D = \frac{1}{2}\varrho^3 c'' c_p \Gamma. \tag{44}$$

Since D is greater than zero for physical thermal state variables $p,T>0 (\Rightarrow \varrho, c_p, c'', u''>0)$ and inflow conditions $u>0$, the regularity of the Jacobian J for meaningful applications is guaranteed.

The average variation of the incoming fifth characteristic variable $\delta\bar{\phi}_5$ is given by

$$\delta\bar{\phi}_5^{(n)} = \mathbf{l}_5^T\big|_{\bar{\mathbf{Q}}^{(n)}} \cdot \left(\delta\bar{\mathbf{Q}}_v\right)_{\mathrm{cal}}^{(n)} = \delta\bar{p}_{\mathrm{cal}}^{(n)} - [\bar{\varrho}(\bar{c'} - \bar{u_0'})]^{(n)} \cdot \delta\bar{u}_{\mathrm{cal}}^{(n)} \tag{45}$$

where the subscript "cal" denotes changes predicted by the flow solver, *i.e.* $\delta\bar{p}_{\mathrm{cal}}^{(n)} = \bar{p}_{\mathrm{cal}}^{(n+1)} - \bar{p}^{(n)}$ where $\bar{p}_{\mathrm{cal}}^{(n+1)}$ represents the predicted static pressure at the actual time step $n+1$ before the boundary values are post-corrected.

When the boundary treatment is simply based on the average one-dimensional characteristic variables, the solution variables $\mathbf{Q}_{v,j}$ at every point $j=1,\ldots,N+1$ of the current circumferential grid line are post-corrected according to

$$\mathbf{Q}_{v,j}^{(n+1)} = \bar{\mathbf{Q}}_v^{(n)} + R|_{\bar{\mathbf{Q}}_v^{(n)}}\, \delta\bar{\boldsymbol{\phi}}^{(n)} \quad \text{with} \quad \delta\bar{\boldsymbol{\phi}} = (\delta\bar{\phi}_1, \delta\bar{\phi}_2, \delta\bar{\phi}_3, \delta\bar{\phi}_4, \delta\bar{\phi}_5)^T, \tag{46}$$

where R represents the matrix of right eigenvectors given in Equation (74).

5.3.2. Axially supersonic inlet

In the case that the flow is axially supersonic at the inlet, all characteristics are incoming wherefore now five boundary conditions need to be given there. In addition to the boundary conditions for the axially subsonic case, the user has to specify the radial distribution of the axial Mach number $\mathrm{Ma}_{\mathrm{x,bc}}(r)$. Since the flow field at the boundary is independent of the downstream flow field, the correct boundary values can be calculated once for all from the user defined boundary conditions. When general equations of state are used, a Newton-Raphson procedure is applied in order to find the correct values of the primitive, viscous variables from the set of nonlinear algebraic equations

$$\begin{gathered} h_0(p_{0,bc},T_{0,bc}) = h(p_{0,bc},T_{0,bc}) = h(p,T) + \frac{1}{2}(u^2+v^2+w^2-(\Omega r)^2), \\ s(p_{0,bc},T_{0,bc}) = s(p,T), \quad \tan\beta_{bc} = \frac{v}{u}, \quad \tan\gamma_{bc} = \frac{w}{u}, \quad \mathrm{Ma}_{\mathrm{x,bc}} = \frac{u}{c(p,T)}. \end{gathered} \tag{47}$$

For ideal gases, the vector of primitive, viscous state variables can be calculated algebraically from the boundary conditions:

$$\begin{aligned} &\mathrm{Ma} = \sqrt{1+\tan^2\beta_{bc}+\tan^2\gamma_{bc}}\cdot\mathrm{Ma}_{\mathrm{x,bc}}, \\ &p = p_{0,bc}\cdot\left(1+\frac{\kappa-1}{2}\mathrm{Ma}^2\right)^{-\frac{\kappa}{\kappa-1}}, \quad T = \frac{T_{0,bc}}{1+\frac{\kappa-1}{2}\mathrm{Ma}^2}, \\ &u = c\cdot\mathrm{Ma}_{\mathrm{x,bc}} = \sqrt{\kappa RT}\cdot\mathrm{Ma}_{\mathrm{x,bc}}, \quad v = u\tan\beta_{bc}, \quad w = u\tan\gamma_{bc}. \end{aligned} \tag{48}$$

5.3.3. Axially subsonic outlet

At an axially subsonic outlet boundary four characteristics are leaving and one characteristic is entering the computational domain. The implementation of the

boundary conditions at outflow is easier than at inflow, because only one boundary condition has to be imposed. As outlet boundary condition for axially subsonic flow, the user has to specify the radial variation of the static pressure $p_{bc}(r)$. Using the residual $R_5 = \bar{p}(r) - p_{bc}(r)$ and linearizing from the current time level yields $R_5^{(n+1)} = R_5^{(n)} + \frac{\partial R_5}{\partial \phi_5}|^{(n)} \delta\bar{\phi}_5^{(n)} := 0$. Calculating the scalar Jacobian $\frac{\partial R_5}{\partial \phi_5}$ and solving the equation for the average change in the fifth characteristic variable leads to

$$\delta\bar{\phi}_5^{(n)} = -\left.\frac{2c''}{c'' + u_0''}\right|_{\bar{\mathbf{Q}}_v^{(n)}} R_5^{(n)}. \tag{49}$$

The variations of the four first characteristics are calculated according to

$$\begin{pmatrix} \delta\bar{\phi}_1 \\ \delta\bar{\phi}_2 \\ \delta\bar{\phi}_3 \\ \delta\bar{\phi}_4 \end{pmatrix}^{(n)} = \begin{pmatrix} \mathbf{l}_1^T \\ \mathbf{l}_2^T \\ \mathbf{l}_3^T \\ \mathbf{l}_4^T \end{pmatrix}_{\bar{\mathbf{Q}}_v^{(n)}} \delta\bar{\mathbf{Q}}_{v,\mathrm{cal}}^{(n)} = \begin{pmatrix} -\frac{1-\varrho h_p}{\varrho h_T} & 0 & 0 & 0 & 1 \\ 0 & 0 & 1 & 0 & 0 \\ 0 & 0 & 0 & 1 & 0 \\ 1 & \varrho(u_0'' + c'') & 0 & 0 & 0 \end{pmatrix}_{\bar{\mathbf{Q}}_v^{(n)}} \begin{pmatrix} \delta\bar{p} \\ \delta\bar{u} \\ \delta\bar{v} \\ \delta\bar{w} \\ \delta\bar{T} \end{pmatrix}^{(n)}_{\mathrm{cal}}. \tag{50}$$

5.3.4. Axially supersonic outlet

When the flow is axially supersonic at the outlet boundary, all characteristics are outgoing, wherefore no boundary condition can be imposed.

5.4. Quasi-three-dimensional non-reflecting boundary conditions

5.4.1. Inlet boundary

In order to obtain a non-reflecting inlet boundary the Giles-condition

$$(\hat{\mathbf{p}}_1, \hat{\mathbf{p}}_2, \hat{\mathbf{p}}_3, \hat{\mathbf{p}}_4)^T \cdot \hat{\mathbf{q}}_k = \mathbf{0} \tag{51}$$

has to be satisfied for each Fourier mode $\hat{\mathbf{q}}_k$ ($k \neq 0$) of the perturbed viscous, primitive variables $\tilde{\mathbf{Q}}_v = \mathbf{Q}_v - \bar{\mathbf{Q}}_v$. By using the relation $L^{-1}\hat{\boldsymbol{\phi}}_k = \hat{\mathbf{q}}_k$, this boundary condition can be expressed in terms of the spatial Fourier modes of the characteristic variables:

$$\begin{pmatrix} 1 & 0 & 0 & 0 & 0 \\ 0 & -v & 0 & -\frac{c''+u-u_0''}{2\varrho c''} & -\frac{c''-u+u_0''}{2\varrho c''} \\ 0 & 0 & 1 & 0 & 0 \\ 0 & -\varrho uc & 0 & -\frac{\beta(c''-u_0'')-vc}{2c''} & -\frac{\beta(c''+u_0'')+vc}{2c''} \end{pmatrix} \hat{\boldsymbol{\phi}}_k = \mathbf{0}. \tag{52}$$

This condition is satisfied trivially when all Fourier components (except the average Fourier mode) of the characteristic variables are zero, *i.e.* $\hat{\boldsymbol{\phi}}_k = 0, \forall k \neq 0$. This shows that one-dimensional characteristic theory alone can be applied to uniform flow fields, such as the far-field of external aerodynamic applications. However, in the general case we have to deal with inhomogeneous flow fields which means that we have to find a way to fulfill the condition stated in Equation (52) non-trivially.

Since the outgoing characteristics do not depend on the boundary conditions but are only given by the interior flow field, they are not manipulable. Thus, the general way to satisfy the condition given in Equation (52) is to define the incoming characteristics as functions of the outgoing ones:

$$\begin{pmatrix} \hat{\phi}_{1,k} \\ \hat{\phi}_{2,k} \\ \hat{\phi}_{3,k} \\ \hat{\phi}_{4,k} \end{pmatrix}^{(n)} := \begin{pmatrix} 0 \\ -\frac{\beta u + vc}{\varrho[c(u^2+v^2)+(c''-u_0'')(uc-v\beta)]} \\ 0 \\ \frac{c(u^2+v^2)-(c''+u_0'')(uc-v\beta)}{c(u^2+v^2)+(c''-u_0'')(uc-v\beta)} \end{pmatrix}_{\bar{\mathbf{Q}}_v^{(n)}} \cdot \hat{\phi}_{5,k}^{(n)}. \tag{53}$$

Since the last condition is formulated in the frequency domain, we have to calculate the local outgoing characteristics by[8]

$$\phi'^{\,(n)}_{5,j} = \mathbf{l}_5^T\big|_{\bar{\mathbf{Q}}_v^{(n)}} \cdot \tilde{\mathbf{Q}}_v^{(n)} = (p_j - \bar{p})^{(n)} + \bar{\varrho}^{(n)}(\overline{u_0''} - \overline{c''})^{(n)} \cdot (u_j - \bar{u})^{(n)}, \quad j = 1,2,\ldots,N \tag{54}$$

and perform a discrete Fourier transformation according to

$$\hat{\phi}_{5,k}^{(n)} = \frac{1}{N} \sum_{j=0}^{N-1} \phi'^{*(n)}_{5,j} \cdot e^{\frac{2\pi \hat{\imath} jk}{N}}, \qquad k = 0,1,\ldots,N-1. \tag{55}$$

N is thereby the number of nodes in the circumferential direction, including the periodic node only once.[9] The set of equidistantly distributed characteristic variables $\phi'^{*}_{5,j}$; $j = 0,\ldots,N$ is obtained from the characteristic variables on the computational grid $\phi'_{5,j}$; $j = 1,\ldots,N+1$ by using spline-interpolation where the endpoints of both sets match, *i.e.* $\phi'^{*}_{5,0} = \phi'_{5,1}$ and $\phi'^{*}_{5,N} = \phi'_{5,N+1} = \phi'_{5,1}$.

The Fourier coefficients of the second characteristic variable are calculated from the Fourier coefficients of the fifth characteristic according to Equation (53)

$$\hat{\phi}_{2,ks}^{(n)} = -\left.\frac{\beta u + vc}{\varrho[c(u^2+v^2) + (c'' - u_0'')(uc - v\beta)]}\right|_{\bar{\mathbf{Q}}_v^{(n)}} \cdot \hat{\phi}_{5,k}^{(n)} = c_{52} \cdot \hat{\phi}_{5,k}^{(n)}, \quad k = 0,1,\ldots,N-1. \tag{56}$$

The correct steady state distribution of the second characteristic variables $c'^{*}_{2,js}$ is obtained from the Fourier coefficients $\hat{\phi}_{2,ks}$ by means of an inverse discrete Fourier transform:

$$\phi'^{*\,(n)}_{2,js} = \sum_{k=0}^{N-1} \hat{\phi}_{2,ks}^{(n)} \cdot e^{-\frac{2\pi \hat{\imath} jk}{N}}, \qquad j = 0,1,\ldots,N-1. \tag{57}$$

Since the Fourier coefficients $\hat{\phi}_{5,k}$ originate from a real function, they possess a conjugate even symmetry with respect to $k = 0$. Due to the definition of β, Equation (39), where k_y corresponds to k used here, the factor c_{52} has the same property, wherefore the inverse discrete Fourier transform (57) for determing the correct steady state distribution of the second characteristics can be simplified to:

$$\phi'^{*}_{2,js} = 2\mathfrak{Re}\left[\sum_{k=1}^{\mathrm{int}(N/2)} \hat{\phi}_{2,ks} \cdot e^{-\frac{2\pi \hat{\imath} jk}{N}}\right], \text{ with } \mathrm{int}(N/2) = \begin{cases} (N-1)/2, & N \text{ odd} \\ N/2, & N \text{ even.} \end{cases} \tag{58}$$

In Equation (58) it was taken into account that the Fourier coefficient $\hat{\phi}_{2,0s}$ equals zero, since the characteristic variables are defined as perturbations from the average state of the last time step n. The distribution of the correct steady state second characteristic variables on the computational grid $\phi'_{2,js}$ are gained from $\phi'^{*}_{2,js}$ again using a cubic interpolation-spline. When the flow is supersonic, but axially subsonic it follows from Equation (39) that the factor c_{52} is real-valued and independent of the

8. Note, even though the left eigenvector $\mathbf{l}_5$ is calculated in dependency of the average state of the last time step, now local variations come into play through the differences $(p_j - \bar{p})^{(n)}$ and $(u_j - \bar{u})^{(n)}$.

9. When a discrete Fourier transformation according to Equation (55) is performed, periodicity of the function $\phi'^{*}_{5,j}$ is assumed implicitly; *i.e.* $\phi'^{*}_{5,j+N} = \phi'^{*}_{5,j}$. Due to the exponential function in Equation (55) this property immediately follows for the Fourier coefficients.

circumferential wave number, wherefore the Giles-condition, Equation (53), can be applied in the time domain and the discrete Fourier transformations can be omitted.

For each node j along the boundary, the local variation of the second characteristic variable $\delta\phi'_{2,j}{}^{(n)}$ is the difference between the correct steady state value $\phi'_{2,js}{}^{(n)}$ and the current value $\phi'_{2,j}{}^{(n)}$:

$$\delta\phi'_{2,j}{}^{(n)} = (\phi'_{2,js} - \phi'_{2,j})^{(n)} = \phi'_{2,js}{}^{(n)} - \mathbf{l}_2^T\big|_{\bar{\mathbf{Q}}_v^{(n)}} \cdot \tilde{\mathbf{Q}}_v^{(n)} = \phi'_{2,js}{}^{(n)} - (v_j - \bar{v})^{(n)}. \tag{59}$$

Since the harmonics of the correct third steady state characteristics are zero, the variation of the third characteristic variable is simply

$$\delta\phi'_{3,j}{}^{(n)} = -\phi'_{3,j}{}^{(n)} = -\mathbf{l}_3^T\big|_{\bar{\mathbf{Q}}_v^{(n)}} \cdot \tilde{\mathbf{Q}}_v^{(n)} = -(w_j - \bar{w})^{(n)}. \tag{60}$$

As noted by Giles [20], an implementation of the last two of the four conditions in Equation (53) would result in a flow field which to first order would have uniform entropy and stagnation enthalpy at each radius. However, the neglected second order effects would introduce variations in entropy and stagnation enthalpy. To avoid this, the steady state corrections of the local first and fourth characteristic variables are obtained from the conditions that the local entropy s_j and the local stagnation enthalpy h_{0j} should match their average values, which is equivalent to drive the residuals

$$R_{1,j} = \bar{\varrho}\bar{T}(s_j - \bar{s}), \qquad R_{4,j} = \bar{\varrho}(h_{0j} - \bar{h}_0) \tag{61}$$

to zero. As shown in [37] for the special case of an ideal gas, a boundary at which constant stagnation enthalpy and entropy are specified is non-reflecting when a Turkel preconditioner [38] is employed, which is of the same type as the one used in the present work. The use of the residuals defined by Equation (61) together with a one-step Newton-Raphson procedure results in the following local changes of the first and fourth characteristic variables:

$$\begin{aligned}
\delta\phi'_{1,j}{}^{(n)} &= -\left.\frac{1}{\varrho h_T}\right|_{\bar{\mathbf{Q}}_v^{(n)}} \cdot R_{1,j}^{(n)}, \\
\delta\phi'_{4,j}{}^{(n)} &= -\left.\frac{2c''}{c'' + u - u_0''}\right|_{\bar{\mathbf{Q}}_v^{(n)}} \cdot [-R_{1,j} + (\bar{\varrho}\bar{v}) \cdot \delta\phi'_{2,j} + (\bar{\varrho}\bar{w}) \cdot \delta\phi'_{3,j} + R_{4,j}]^{(n)}.
\end{aligned} \tag{62}$$

Now that the local variations of the incoming characteristic variables have been determined, they are added to the average changes according to

$$\delta\phi_{i,j} = \sigma(\delta\phi'_{i,j} + \delta\bar{\phi}_i), \quad i = 1, \ldots, 4, \tag{63}$$

where the relaxation factor σ is chosen to $1/N$. The total variation of the fifth characteristic variable $\delta\phi_{5,j}^{(n)}$ is calculated as

$$\delta\phi_{5,j}^{(n)} = \mathbf{l}_5^T\big|_{\bar{\mathbf{Q}}_v^{(n)}} (\mathbf{Q}_{v,j}^{(n+1)} - \mathbf{Q}_{v,j}^{(n)}) = p_{j,\mathrm{cal}}^{(n+1)} - p_j^{(n)} + \bar{\varrho}(\overline{u_0''} - \overline{c''})^{(n)}(u_{j,\mathrm{cal}}^{(n+1)} - u_j^{(n)}). \tag{64}$$

Finally, the total characteristic changes are transformed back into changes of the viscous, primitive variables and the state vector is updated according to

$$\mathbf{Q}_{v,j}^{(n+1)} = \mathbf{Q}_{v,j}^{(n)} + R|_{\bar{\mathbf{Q}}_v^{(n)}} \cdot \delta\boldsymbol{\phi}_j^{(n)} =$$

$$= \begin{pmatrix} p_j \\ u_j \\ v_j \\ w_j \\ T_j \end{pmatrix}^{(n)} + \begin{pmatrix} 0 & 0 & 0 & \frac{c''-u_0''}{2c''} & \frac{c''+u_0''}{2c''} \\ 0 & 0 & 0 & \frac{1}{2\varrho c''} & -\frac{1}{2\varrho c''} \\ 0 & 1 & 0 & 0 & 0 \\ 0 & 0 & 1 & 0 & 0 \\ 1 & 0 & 0 & \frac{1-\varrho h_p}{\varrho h_T}\frac{c''-u_0''}{2c''} & \frac{1-\varrho h_p}{\varrho h_T}\frac{c''+u_0''}{2c''} \end{pmatrix}_{\bar{\mathbf{Q}}_v^{(n)}} \begin{pmatrix} \delta\phi_{1,j} \\ \delta\phi_{2,j} \\ \delta\phi_{3,j} \\ \delta\phi_{4,j} \\ \delta\phi_{5,j} \end{pmatrix}^{(n)} . \quad (65)$$

5.4.2. Outlet boundary

The Giles condition for a non-reflecting spatial distribution of the perturbed primitive, viscous variables at the outlet boundary can be expressed as $\hat{\mathbf{p}}_5^T \cdot \hat{\mathbf{q}}_k = (\beta, \varrho vc, -\varrho uc, 0, 0) \cdot \hat{\mathbf{q}}_k = 0$, or in terms of the characteristic variables as:

$$\left(0, -\varrho uc, 0, \frac{1}{2c''}[\beta(c''-u_0'')+vc], \frac{1}{2c''}[\beta(c''+u_0'')-vc]\right) \cdot \hat{\boldsymbol{\phi}}_k = 0 \quad (66)$$

for all Fourier modes $k \neq 0$. The Fourier modes of the ingoing fifth characteristic variable are defined as functions of the Fourier modes of the outgoing second and fourth characteristics according to

$$\hat{\phi}_{5,ks}^{(n)} := \frac{2\varrho ucc''}{\beta(c''+u_0'')-vc}\bigg|_{\bar{\mathbf{Q}}_v^{(n)}} \cdot \hat{\phi}_{2,k}^{(n)} - \frac{\beta(c''-u_0'')+vc}{\beta(c''+u_0'')-vc}\bigg|_{\bar{\mathbf{Q}}_v^{(n)}} \cdot \hat{\phi}_{4,k}^{(n)}, \quad k = 0,1,\ldots,N-1. \quad (67)$$

The Fourier modes $\hat{\phi}_{2,k}$ and $\hat{\phi}_{4,k}$ are computed by first calculating $\phi'_{2,j}$ and $\phi'_{4,j}$ from the following relations:

$$\begin{aligned} {\phi'_{2,j}}^{(n)} &= \mathbf{l}_2^T\big|_{\bar{\mathbf{Q}}_v^{(n)}} \cdot (\mathbf{Q}_{v,j} - \bar{\mathbf{Q}}_v)^{(n)} = (v_j - \bar{v})^{(n)}, \\ {\phi'_{4,j}}^{(n)} &= \mathbf{l}_4^T\big|_{\bar{\mathbf{Q}}_v^{(n)}} \cdot (\mathbf{Q}_{v,j} - \bar{\mathbf{Q}}_v)^{(n)} = (p_j - \bar{p})^{(n)} + \bar{\varrho}^{(n)}(\overline{u_0''} + \overline{c''})^{(n)} \cdot (u_j - \bar{u})^{(n)}. \end{aligned} \quad (68)$$

Then these quantities are transferred onto an equidistant grid and Fourier transformations of the spatially equidistantly distributed characteristic variables ${\phi'^*_{2,j}}^{(n)}$ and ${\phi'^*_{4,j}}^{(n)}$ are performed according to

$$\hat{\phi}_{2,k}^{(n)} = \frac{1}{N}\sum_{j=0}^{N-1} {\phi'^*_{2,j}}^{(n)} \cdot e^{\frac{2\pi \hat{\imath} jk}{N}}, \qquad \hat{\phi}_{4,k}^{(n)} = \frac{1}{N}\sum_{j=0}^{N-1} {\phi'^*_{4,j}}^{(n)} \cdot e^{\frac{2\pi \hat{\imath} jk}{N}}, \qquad k = 0,1,\ldots,N-1. \quad (69)$$

Using the simplification due to conjugate even symmetry of the Fourier coefficients $\hat{c}_{5,ks}$ with respect to $k = 0$ allows the non-reflecting steady state values $c'^*_{5,js}$ for the incoming fifth characteristic variables to be written as:

$${\phi'^*_{5,js}}^{(n)} = \sum_{k=1}^{\mathrm{int}(N/2)} \hat{\phi}_{5,ks}^{(n)} \cdot e^{-\frac{2\pi \hat{\imath} jk}{N}}, \qquad j = 0,1,\ldots,N-1. \quad (70)$$

With ${\phi'_{5,j}}^{(n)}$ calculated to:

$${\phi'_{5,j}}^{(n)} = \mathbf{l}_5^T\big|_{\bar{\mathbf{Q}}_v^{(n)}} \tilde{\mathbf{Q}}_{v,j}^{(n)} = p_j^{(n)} - \bar{p}^{(n)} + \bar{\varrho}^{(n)}(\overline{u_0''} - \overline{c''})^{(n)}(u_j^{(n)} - \bar{u}^{(n)}) \quad (71)$$

and the average variation of the fifth characteristic variable $\delta\bar{\phi}_5^{(n)}$ given by Equation (49) one obtains the total variation as:

$$\delta\phi_{5,j}^{(n)} = \sigma(\delta\bar{\phi}_5^{(n)} + {\phi'_{5,js}}^{(n+1)} - {\phi'_{5,j}}^{(n)}). \quad (72)$$

The total variations of the first four characteristic variables are determined directly by:

$$\begin{pmatrix}\delta\phi_{1,j}\\ \delta\phi_{2,j}\\ \delta\phi_{3,j}\\ \delta\phi_{4,j}\end{pmatrix}^{(n)} = \begin{pmatrix}\mathbf{l}_1^T\\ \mathbf{l}_2^T\\ \mathbf{l}_3^T\\ \mathbf{l}_4^T\end{pmatrix}_{\bar{\mathbf{Q}}_v^{(n)}} \cdot \begin{pmatrix}\delta p_j\\ \delta u_j\\ \delta v_j\\ \delta w_j\\ \delta T_j\end{pmatrix}^{(n)}_{\text{cal}} =$$

$$= \begin{pmatrix} -\frac{1-\varrho h_p}{\varrho h_T} & 0 & 0 & 0 & 1\\ 0 & 0 & 1 & 0 & 0\\ 0 & 0 & 0 & 1 & 0\\ 1 & \varrho(u_0''+c'') & 0 & 0 & 0\end{pmatrix}_{\bar{\mathbf{Q}}_v^{(n)}} \cdot \begin{pmatrix} p_{j,\text{cal}}^{(n+1)} - p_j^{(n)}\\ u_{j,\text{cal}}^{(n+1)} - u_j^{(n)}\\ v_{j,\text{cal}}^{(n+1)} - v_j^{(n)}\\ w_{j,\text{cal}}^{(n+1)} - w_j^{(n)}\\ T_{j,\text{cal}}^{(n+1)} - T_j^{(n)}\end{pmatrix} \tag{73}$$

Finally, the total characteristic changes are transformed back into changes of the viscous, primitive variables and the state vector is updated according to Equation (65).

5.4.3. Adjacent solid walls

In calculations of viscous flow, the boundary points that lie in one of the flow boundary planes as well as on a solid wall require a special treatment.[10] First, the solid wall boundary conditions are imposed by setting all components of the velocity vector to zero. At the inlet boundary static pressure and temperature are set to the user specified total values. At the outlet boundaries the pressure is set to the corresponding user defined value, whereas the temperature is obtained by a linear extrapolation of the temperature in the radial direction.

5.4.4. Mixing planes

In steady multistage calculations of turbomachinery, mixing planes are used for coupling different frames of reference and transferring circumferentially averaged data from one row to another. The mixing planes used in ITSM3D apply the one-dimensional characteristic theory to enforce the condition that mass, impulse and energy are conserved across the interface. Reflections at these boundaries are prevented applying the Giles condition, Equation (35). Since a mixing plane in principle represents an inlet boundary coupled with an upstream outlet boundary, the extension of the non-reflecting inlet and outlet boundaries to non-reflecting mixing planes is straightforward.

6. Computational results

6.1. Ni-Bump test case

To demonstrate that the preconditioned scheme is able to calculate a configuration efficiently and accurately over a broad Mach number range, at first results from the calculation of the Ni-Bump test case given in [39] are presented. In this test case the internal inviscid, two-dimensional flow through a parallel channel having a 4.2%

10. The coefficient c_{52} defined in Equation (56) is given by $c_{52} = \frac{\hat{i}}{2\varrho u}$ for $v = 0$ and $u \to 0$, showing that the non-reflecting boundary treatment in combination with the preconditioning is singular at walls.

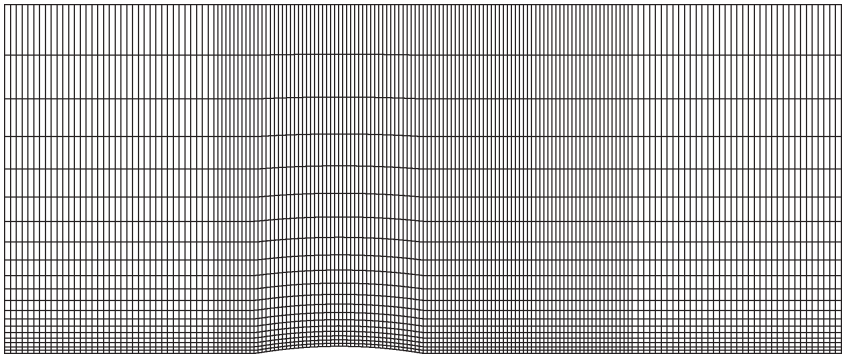

Figure 1. Computational grid for the Ni-Bump test case

thick circular bump on the lower wall is considered. The computational grid is shown in Figure 1 and consists of $177 \times 3 \times 21$ grid points.

The calculations were initialized setting the axial velocity of every grid point to $\mathrm{Ma} = 0.6$ and they were run until the continuity residual had decreased by four orders of magnitude. We were performing calculations using only 4 Byte real variables in our computations. When initializing the flow field with the isentropic Mach number given by the inlet total pressure and outlet static pressure, which of course would be a more physical choice, the residuals were only decreasing by three orders in magnitude before machine zero was encountered. In future work we will split the pressure variable into a gauge pressure and a perturbed pressure, thereby reducing round-off errors due to small pressure variations and avoiding the use of double precision arithmetics.

Table 1 shows the calculations performed with preconditioning (PC) and without preconditioning (NonPC) and the number of iterations N that were necessary before convergence was achieved.

Table 1. Number of iterations N needed for convergence in dependency of the isentropic Mach number $\mathrm{Ma}_{\mathrm{is}}$

$\mathrm{Ma}_{\mathrm{is}}$	N (PC)	N (NonPC)
0.013	3180	8920
0.037	3330	7770
0.084	3750	5620
0.850	2690	2910

In the case of an isentropic Mach number $\mathrm{Ma}_{\mathrm{is}} = 0.85$ the original boundary conditions [39] were used and the flow is transonic. The solutions obtained with the original and the preconditioned scheme are plotted in Figure 2a and Figure 2b, respectively. The calculated flowfields are nearly identical, which shows that the shock capturing property of the original scheme is retained when preconditioning is used. For this case, the preconditioned scheme is only marginally faster than the original scheme.

When the preconditioned scheme was used at the other Mach number cases, convergence was always achieved within 4000 iterations. As expected, the necessary number of iterations using the original scheme is increasing with decreasing Mach

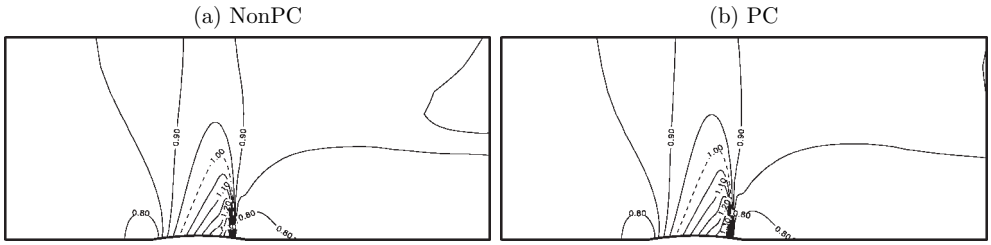

Figure 2. Calculated Mach number contours of the transonic Ni-Bump test case ($\mathrm{Ma_{is}} = 0.85$) using the non-preconditioned (NonPC) and the preconditioned (PC) scheme

number. However, a more serious problem that accrues when using the original scheme is the deterioration of accuracy with decreasing Mach number.

When looking at Figure 3a, where the lines of constant static pressure of the solution obtained with the original scheme are plotted, it is hard to believe that the residual has fallen by four orders of magnitude, which is sufficient for obtaining interpretable, physical results in most other cases. In fact, using in total 16750 iterations and thereby driving the residuals to machine zero, results in a significant change of the solution, Figure 3b.

On the contrary, the solution of the preconditioned scheme depicted in Figure 3e, remains unchanged after the residual has fallen by three orders of magnitude. The obtained flow field is the expected one, except for the wiggles in the inlet and outlet area of the solution. These wiggles are due to the fact that the solution there does not change within the first six decimals, wherefore random distributed round-off errors come into play when the isolines are constructed.

When comparing the Mach number distributions obtained with the different schemes, Figure 3d and Figure 3f, it is apparent that the original scheme is much more diffusive than the preconditioned scheme, since the former produces a long tail after the Bump with reduced Mach numbers in the solution. When zooming in at the flow field over the bump, Figure 3g–j, it becomes evident that accuracy of the solution scheme is only preserved at low Mach numbers when preconditioning is used.

6.2. 1.5 stage low-speed test rig

In order to verify that the presented scheme is able to simulate low-speed multistage turbomachinery efficiently, we now consider the simulation of the flow in a 1.5 stage axial air turbine, where the Mach number ranges from $\mathrm{Ma} = 0.05 - 0.15$ in the main flow. It will be shown that on coarse grids the secondary flow effects are only captured when preconditioning is used.

The turbine considered is operated in a test rig at the Ruhr-Universität Bochum where extensive steady-state measurements have been carried out [24]. It consists of two identical stator blade rows and a rotor with a labyrinth seal on the shroud in between. Figure 4a shows a meridional view of the turbine and its measurement planes. An azimuthal cut through the turbine with midspan velocity triangles and definitions of the flow angles are shown in Figure 4b. The test rig is operated at peak efficiency condition (design condition) with a rotor speed of $n = 500\,\mathrm{rpm}$. At two different clearance heights $s = 1\,\mathrm{mm}$ ($s/D = 0.07\%$) and $s = 3\,\mathrm{mm}$ the flow fields in the planes M1, M2 and M3 were measured with a pneumatic 5-hole probe at defined inlet

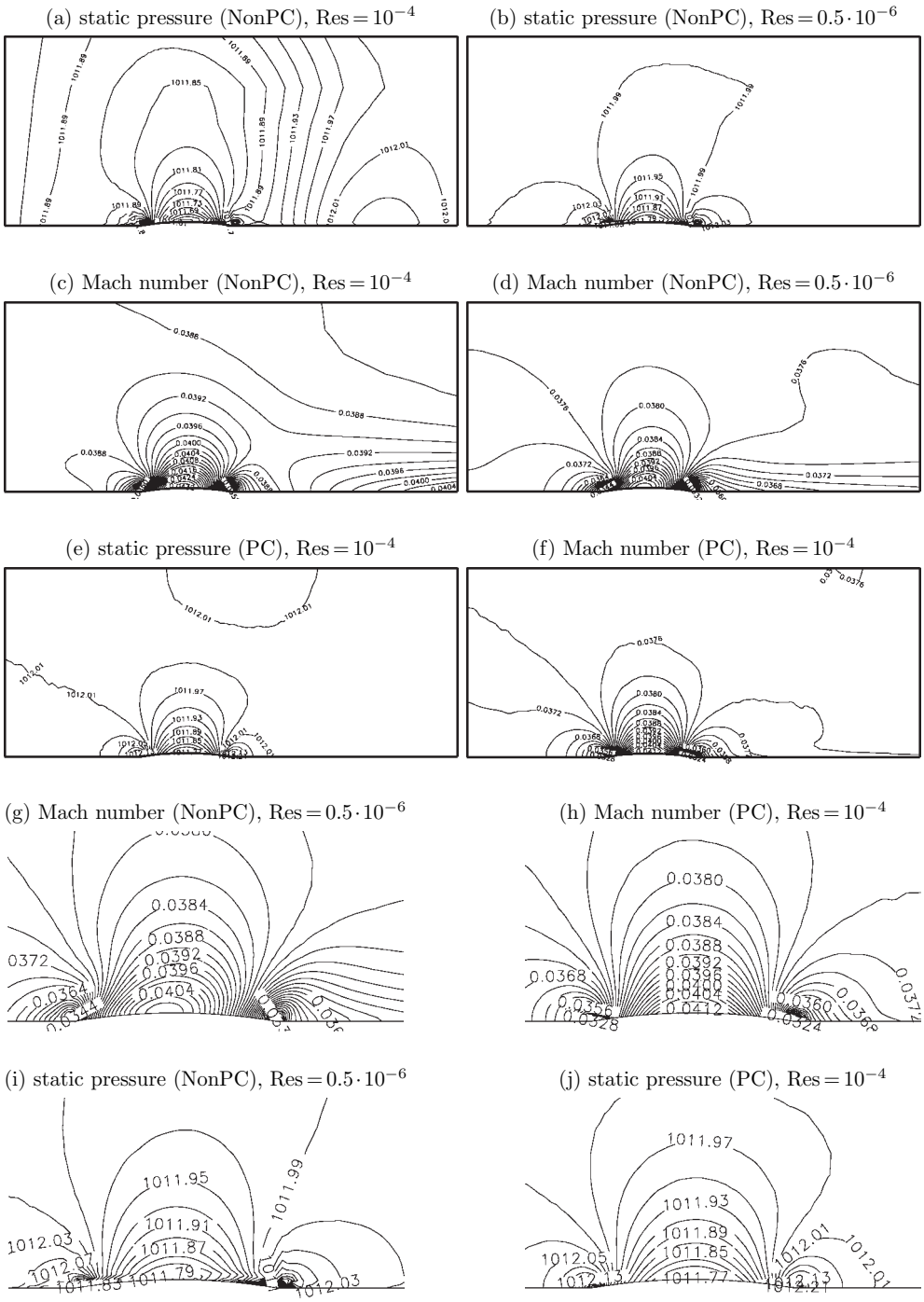

Figure 3. Mach number and static pressure contours of the flow calculated in the subsonic Ni-Bump test case ($Ma_{is} = 0.037$) using the preconditioned (PC) and the non-preconditioned scheme (NonPC)

and outlet conditions in M0 and A1, respectively. A detailed description of the test rig and the measurements carried out in Bochum can be found in [33]. Since leakage flow effects are beyond the scope of this paper, we were not modeling the labyrinth seal. We will therefore compare the computational results with the measurements for the clearance height of 1 mm, since in this case the leakage flow effects are minimal.

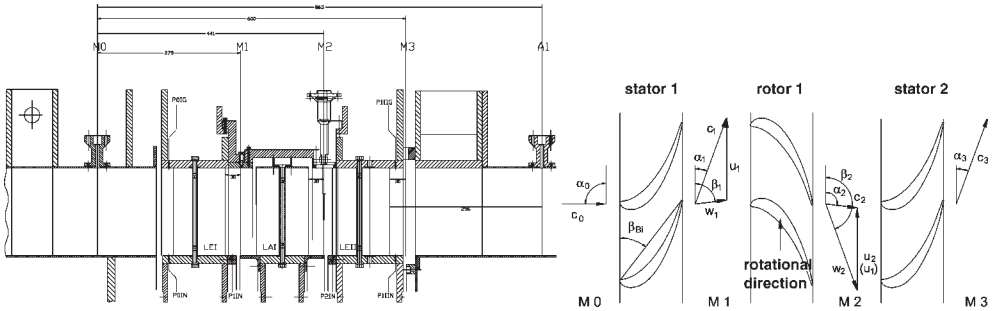

Figure 4. Turbine geometry; (a) measurement planes; (b) blading and angle definitions

The 1.5 stage axial turbine was discretized using a block-structured grid. In Figure 5 the block topology and the positions of the mixing planes are shown. The numerical grids used consist of 235000 grid points in total; the first stator was discretized using $61\times25\times33$ nodes.

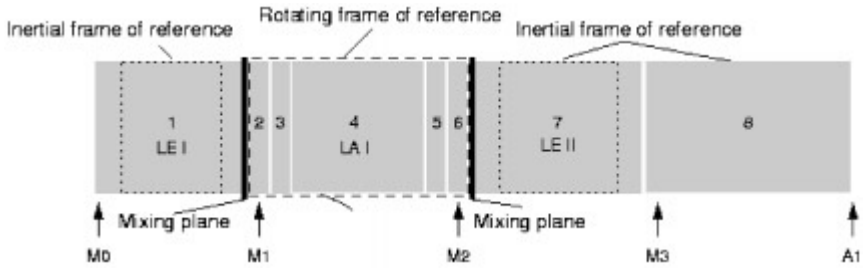

Figure 5. Block topology and the position of the mixing planes

The first simulation was performed using the preconditioned scheme described in this paper until the residuals had fallen by three orders of magnitude on the finest grid level and the mass flow rates had reached constant values. With CFL=2 and $k^{(4)} = 0.05$, using four multiple-grid levels and an impulsive start, convergence was achieved within 9000 iterations, see Figure 6a for the convergence history. Using the flow field obtained with the preconditioned scheme as an initial solution the flow field was also calculated with the original scheme with the same parameters of the dissipation scheme and an unaltered CFL number.

As seen by Figure 6b the original scheme needs 16000 iterations in order to achieve a residual drop by three orders of magnitude. Apparently, the preconditioned scheme is not only converging faster but also more smoothly.

In Figure 7a and Figure 7b the static pressure contours of the solution computed with the preconditioned (PC) and the original scheme (NonPC) are plotted in the

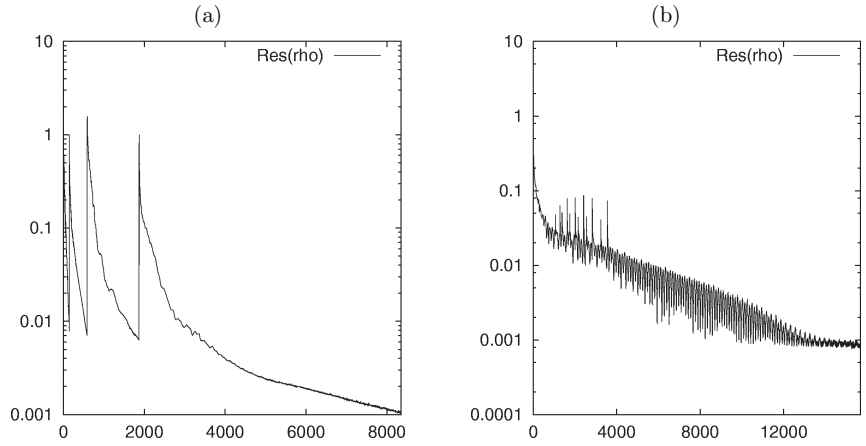

Figure 6. Convergence history: (a) impulsive start with the preconditioned scheme using four multiple-grid levels; (b) original scheme where the converged solution obtained with the preconditioned scheme was used for initialization

azimuthal plane at midspan, respectively. Details of this plots are shown in Figure 8. The original scheme produces unphysical wiggles in the solution, especially at the leading edges of the blades. Further, the isobars of the computed flow field are not perpendicular to the boundary layers.[11] In contrast to this, the preconditioned scheme produces smooth and physical solutions in all regions of the flow. Furthermore, from Figure 8c it is apparent that the boundary conditions for the preconditioned scheme are non-reflecting.

In Figure 9 the calculated circumferentially averaged velocities and yaw angles are compared to measurement data. As seen by the circumferentially averaged axial velocities, both the preconditioned scheme and the original one are underpredicting the axial velocities. While a mass flow of 13.04kg/s was measured, the preconditioned scheme predicts a mass flow of 12.4kg/s, whereas in the simulation with the original scheme a mass flow rate of 12.0kg/s was obtained. Since circumferentially averaged yaw angles in M1 are predicted well by both schemes, the averaged circumferential velocities are consequently also underpredicted.

The measured circumferentially averaged velocities in M2, depicted in Figure 10, reveal that there is a reduced mass flow in the hub region of the rotor, since the hub-side passage vortex causes an overturning of the main flow. While the preconditioned solver captures the tendencies of the secondary flow, the original scheme completely fails to reproduce the secondary effects. Further, with the exception of flow in the casing region in M2, were the rudimentary leakage flow is entering the main flow, the preconditioned solver predicts the averaged circumferential velocities fairly well. Conformal with the findings of [40], we know from previous results [41] that by using enough grid points and lowering the artificial damping parameter $k^{(4)}$, some of the

11. Previous work showed that using finer grids leads to sleeker isobars in the main flow. However, the use of finer grid does not alleviate the problem of solution decoupling in the boundary layers, on the contrary. With a finer discretization of the boundary layer, the Mach number of the points nearest to the wall is decreasing, whereby the low Mach number deficiencies in the neighbourhood of the wall becomes pronounced.

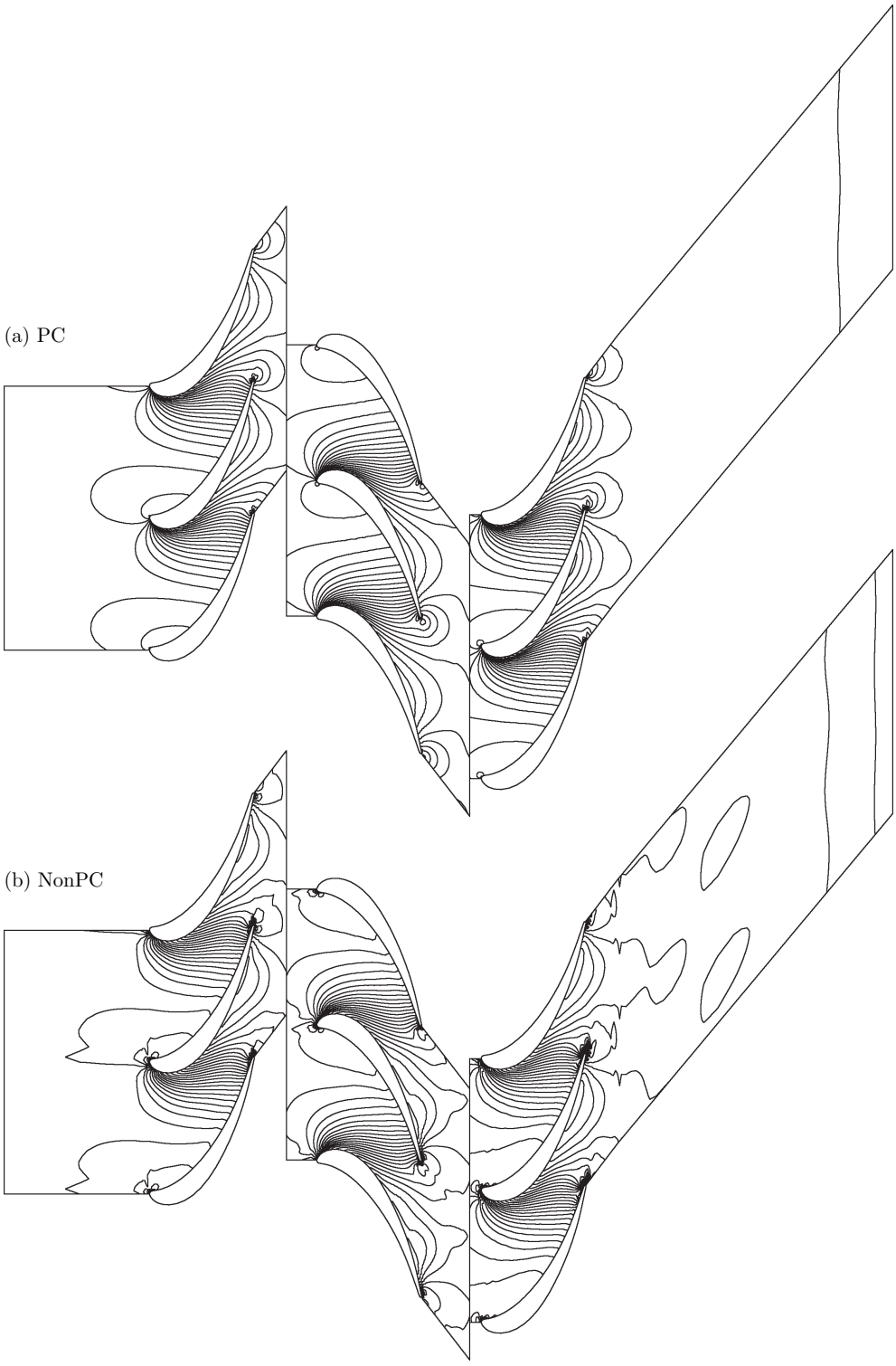

Figure 7. Lines of constant pressure computed with the preconditioned (PC) and the original scheme (NonPC)

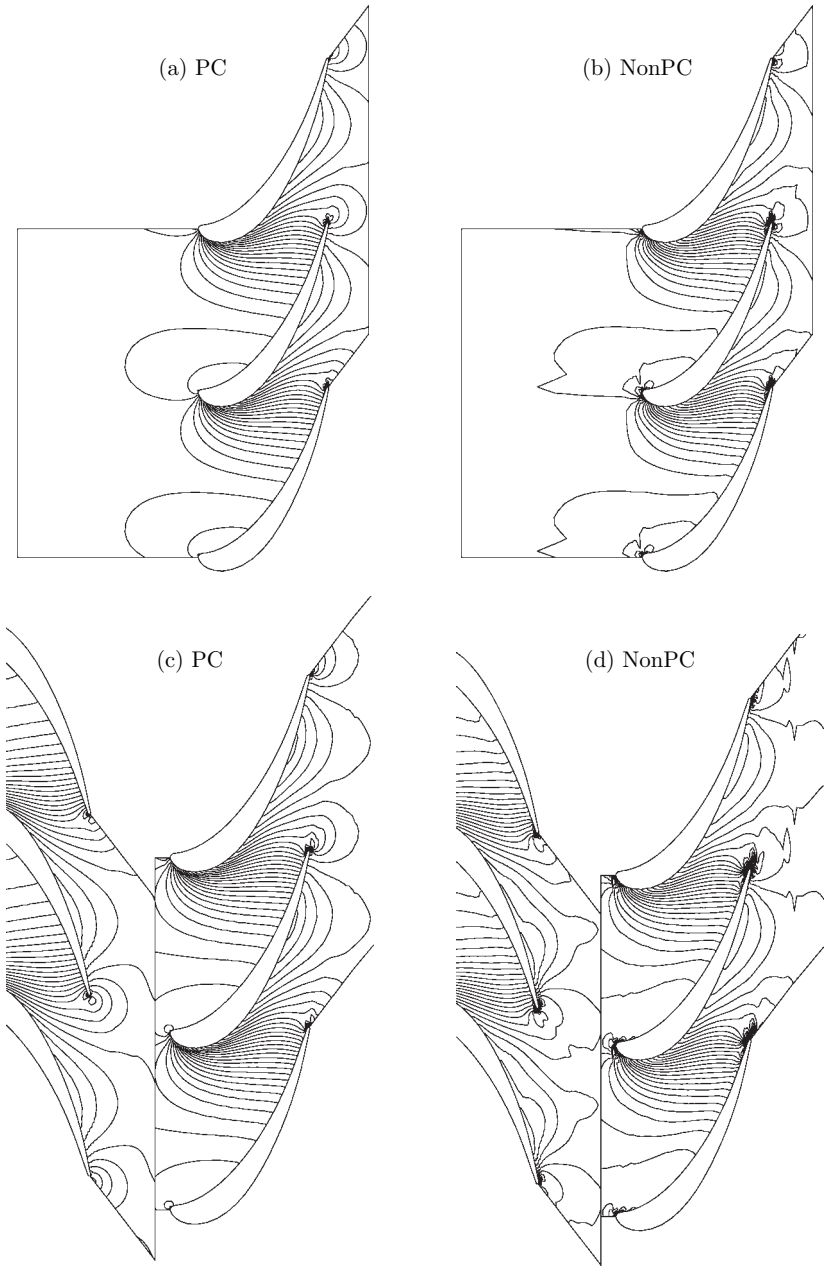

Figure 8. Lines of constant pressure computed with the preconditioned (PC) and the original scheme (NonPC)

deficiencies of using a compressible code for low Mach numbers flows can be diminished. However, the use of 3.2 million grid points as in [41] instead of the 235000 grid points used here, is not practicable when also taking into account that the original scheme exhibits a slower convergence rate. The results presented here clearly show the need for preconditioning when simulating low Mach number flow in multistage turbomachinery.

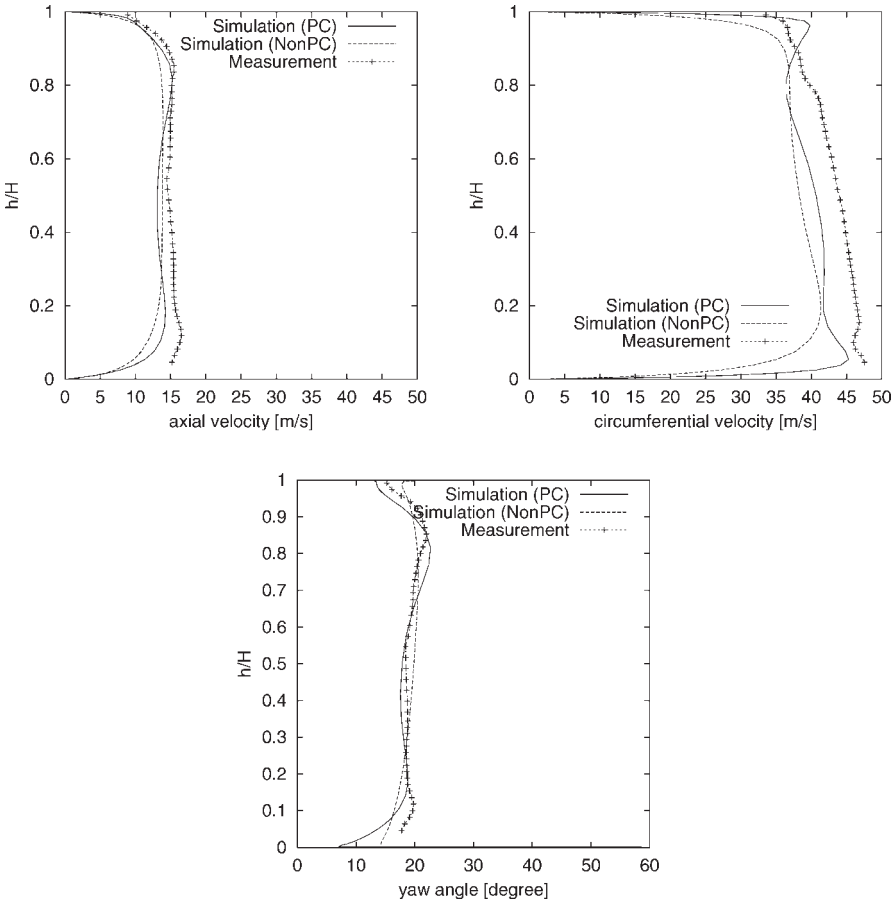

Figure 9. Circumferentially averaged velocities and yaw angles over the relative channel height h/H in the measurement plane M1 (30mm behind stator I)

6.3. Isolated vane

The preconditioning method described in the previous chapter was first used with the original boundary conditions for the unscaled Navier-Stokes equations. However, as previously noted, this was often leading to instabilities in the vicinity of the inlet boundaries, outlet boundaries, and the mixing planes. In order to demonstrate the effectiveness of the novel boundary treatment at low Mach numbers, in the following the results from the simulations of the flow through the second stator row of the test rig considered in Chapter 6.2 using different boundary conditions will be presented. To be concrete, the original quasi-three-dimensional, non-reflecting boundary treatment is compared with the corresponding boundary treatment for the preconditioned Navier-Stokes equations. The latter boundary conditions were also used without applying the non-reflecting correction, thereby basing this boundary treatment on the averaged characteristics only.

As boundary conditions an inlet total pressure of 1013mbar and an outlet static pressure of 1000mbar were specified. The difference of 13mbar corresponds approximately to the pressure difference over the second stator of the last test case.

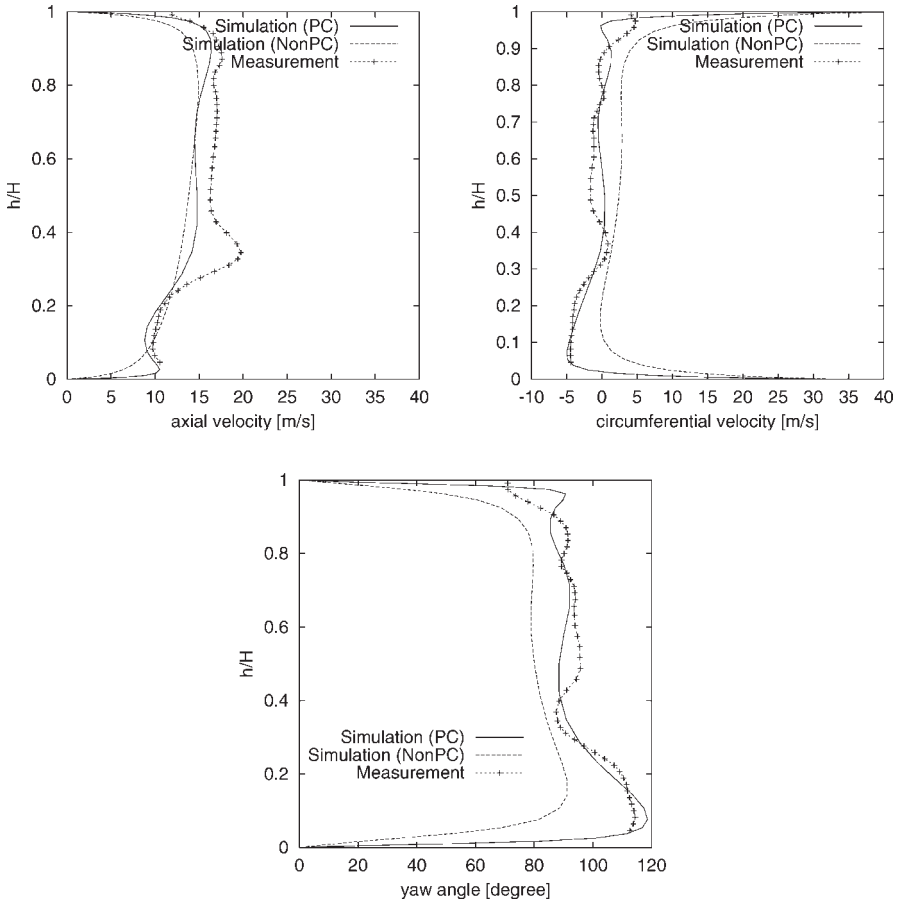

Figure 10. Circumferentially averaged velocities and yaw angles over the relative channel height h/H in the measurement plane M2 (30mm behind rotor)

The calculations were run on a grid consisting of $49 \times 25 \times 33$ grid points. The flow solver was run with CFL=2.0, $k^{(4)} = 0.05$, and $\epsilon_{pgr} = 1.0$ while using three multiple-grid levels for convergence acceleration. As a switching criterion from one multigrid level to the next, a relative residual drop by two orders of magnitude was chosen.

The computations with boundary conditions based on the one-dimensional characteristics of the preconditioned scheme diverged at the finest grid level. In order to increase the robustness of the scheme the parameter ϵ_{pgr} was raised to $\epsilon_{pgr} = 10.0$. This did not lead to instability, but the residual stagnated after a drop by 2.5 orders of magnitude on the finest grid level. In Figure 11a the calculated flowfield is depicted. It reveals unphysical reflections at the boundaries.

The original boundary conditions did not lead to instability, but with $\epsilon_{pgr} = 1.0$, the residual did not decrease at all at the coarsest grid level. Setting ϵ_{pgr} to $\epsilon_{pgr} = 10.0$ led to a residual drop by 1.5 orders of magnitude on the finest grid level. From the computed flowfield in Figure 11b the reason for the inhibited convergence can be seen: The lines of constant pressure are wiggling at the boundary, revealing a poor boundary treatment. The deficiency in the boundary treatment is dependent on the

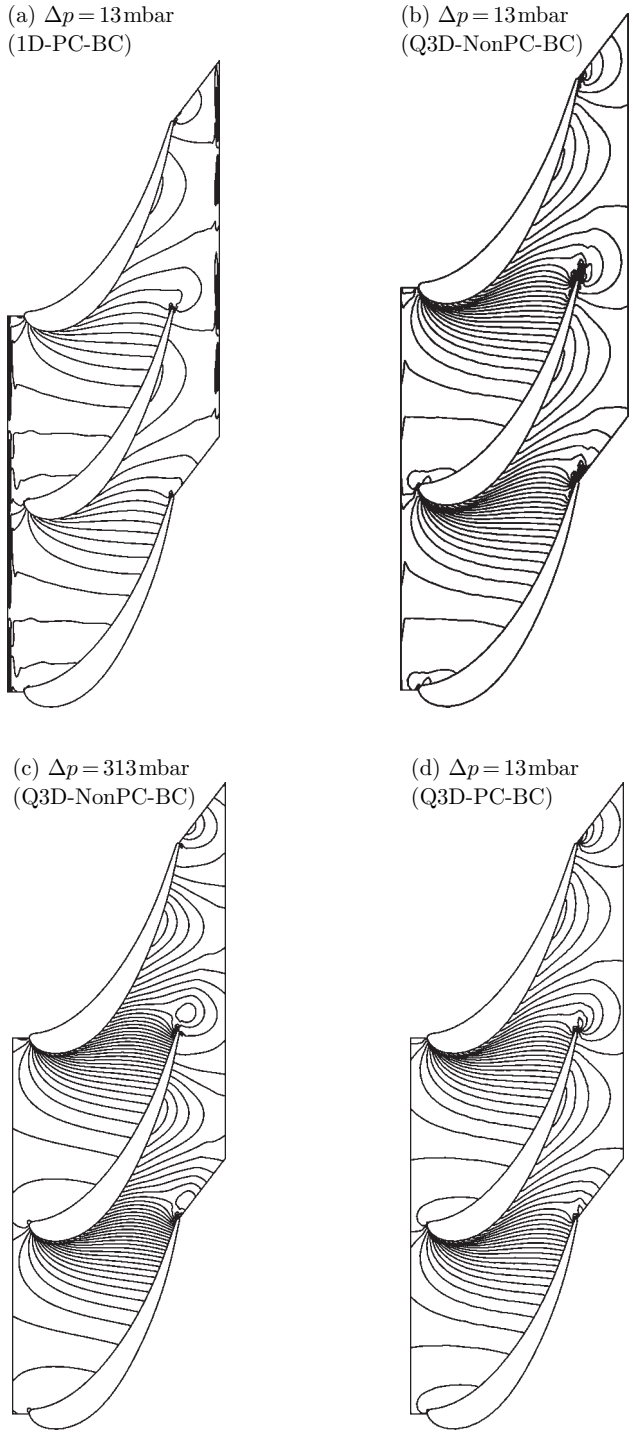

Figure 11. Lines of constant pressure of the computed flow fields using different boundary conditions

Mach number. By lowering the outlet pressure to 700 mbar ($\mathrm{Ma_{is}} = 0.6$), the solution converged and the original boundary condition seemed to be non-reflecting for this case, *cf.* Figure 11c.

When using the novel boundary conditions the residuals dropped by three orders of magnitude and a physical flow field was obtained for both $\epsilon_{pgr} = 1.0$ and $\epsilon_{pgr} = 10.0$. In Figure 11d the isolines of the static pressure calculated with $\epsilon_{pgr} = 1.0$ are depicted. When accumulating the residual drops of all levels, the residual dropped 7 orders of magnitude in total.

The problems encountered when a reflective or a non-consistent boundary treatment is used, are getting even worse when lowering the Mach number. Furthermore, since setting ϵ_{pgr} to a value greater than unity is nothing else than taking the preconditioning back, the presented results show that the new boundary conditions are indispensable, when low Mach number flow is to be computed.

7. Conclusions

A preconditioned solution scheme for the computation of compressible flow in turbomachinery at arbitrary Mach numbers was presented. The governing equations, the finite volume discretization and the solution scheme were described and details of the preconditioning method were given. Since preconditioning changes the characteristics of the governing equations, a modification of the original quasi-three-dimensional non-reflecting boundary conditions according to Giles and Saxer was necessary. A derivation of the appropriate boundary conditions for the presented preconditioned scheme was performed for general equations of state. The resulting equations and the main aspects of the novel boundary treatment derived and implemented in the solution scheme were given.

To demonstrate accuracy and efficiency of the method several test cases were presented. Varying the isentropic Mach number in the Ni-Bump test case from 0.013 to 0.85 showed that with preconditioning Mach number independent convergence rates can be obtained. While preconditioning does not impair the shock capturing property of the original solution scheme, the accuracy of the solution scheme is preserved at low Mach numbers only when preconditioning is used.

In the second test case the turbulent flow in a 1.5 stage low-speed test rig was computed. Without the use of preconditioning unphysical wiggles in the pressure field were observed. On the coarse grid used, the original scheme completely failed to reproduce the secondary flow effects measured, whereas the preconditioned solver captured the tendencies of the secondary flow effects and produced smooth solutions in all regions of the flow.

In the last test case the flow through an isolated vane using different boundary conditions in conjunction with the preconditioned scheme was simulated. The original boundary conditions developed for the unscaled Navier-Stokes equations could be used in the case of an isentropic Mach number of $\mathrm{Ma_{is}} = 0.6$. However, the use of these unmodified boundary conditions led to instabilities and an unphysical pressure distribution in the vicinity of the boundaries at low Mach numbers. Obviously, the original boundary treatment can only be used at compressible flow conditions, where the preconditioned equations turn to the physical ones. The benefit of the novel

boundary conditions presented in this paper is given by the fact that they were the only ones that led to stable integration and non-reflecting boundaries over a broad Mach number range.

Acknowledgements

The authors would like to thank their colleagues P. Gerkens, F. Delhopital, and U. Seybold for the helpful comments and suggestions regarding this paper.

8. Appendix

8.1. Left and right eigenvectors (1D)

For the one-dimensional case with $k_x/\omega = 1$, $k_y = 0$, $k_z = 0$ and $\varrho'_T = \varrho_T$, $h'_p = 1 - \varrho h_p$, $h'_T = h_T$ the eigenvector matrices $L = (\mathbf{l}_1, \mathbf{l}_2, \mathbf{l}_3, \mathbf{l}_4, \mathbf{l}_5)^T$ and $R = (\mathbf{r}_1, \mathbf{r}_2, \mathbf{r}_3, \mathbf{r}_4, \mathbf{r}_5)$ of the matrix $\check{A}_\Gamma$ defined in Equation (29) are given by

$$L = \begin{pmatrix} -\frac{1-\varrho h_p}{\varrho h_T} & 0 & 0 & 0 & 1 \\ 0 & 0 & 1 & 0 & 0 \\ 0 & 0 & 0 & 1 & 0 \\ 1 & \varrho(u_0'' + c'') & 0 & 0 & 0 \\ 1 & \varrho(u_0'' - c'') & 0 & 0 & 0 \end{pmatrix}, \quad R = \begin{pmatrix} 0 & 0 & 0 & \frac{c''-u_0''}{2c''} & \frac{c''+u_0''}{2c''} \\ 0 & 0 & 0 & \frac{1}{2\varrho c''} & -\frac{1}{2\varrho c''} \\ 0 & 1 & 0 & 0 & 0 \\ 0 & 0 & 1 & 0 & 0 \\ 1 & 0 & 0 & \frac{1-\varrho h_p}{\varrho h_T}\frac{c''-u_0''}{2c''} & \frac{1-\varrho h_p}{\varrho h_T}\frac{c''+u_0''}{2c''} \end{pmatrix}. \quad (74)$$

The scaled velocities u'', u_0'' and c'' are defined as:

$$\begin{aligned} u'' &= \frac{1}{2}u(1 + \frac{d}{d'}), \\ u_0'' &= \frac{1}{2}u(1 - \frac{d}{d'}), \\ c'' &= \frac{1}{2}\sqrt{u^2(1 - \frac{d}{d'})^2 + 4\frac{\varrho h_T}{d'}} = \sqrt{u_0''^2 + c'^2}, \end{aligned} \quad (75)$$

with the quantities d and d' given in Equation (7). The left eigenvectors $\mathbf{l}_i$, $i = 1, 2, \ldots, 5$ and right eigenvectors $\mathbf{r}_i$, $i = 1, 2, \ldots, 5$ are defined by

$$(\mathbf{l}_i)^T(\check{A}_\Gamma - \omega_i I) = \mathbf{0} \quad \text{and} \quad (\check{A}_\Gamma - \omega_i I)\mathbf{r}_i = \mathbf{0}, \quad (76)$$

respectively. With the eigenvalues

$$\omega_{1,2,3} = u, \qquad \omega_{4,5} = \frac{1}{2}u\left(1 + \frac{d}{d'}\right) \pm \frac{1}{2}\sqrt{u^2\left(1 - \frac{d}{d'}\right)^2 + 4\frac{\varrho h_T}{d'}} \quad (77)$$

the eigenvectors are sorted according to the convention that the first four always correspond to positive eigenvalues when the axial velocity u is positive:

$$L = \begin{pmatrix} \mathbf{l}_1(\omega_1)^T \\ \ldots \\ \mathbf{l}_5(\omega_5)^T \end{pmatrix}, \quad R = (\mathbf{r}_1(\omega_1), \ldots, \mathbf{r}_5(\omega_5)). \quad (78)$$

These matrices are valid for general equations of state including the incompressible case with $\varrho = \text{const.}$ and $d = 0$. Note that in the case of no preconditioning, $d = d'$, from which $u = u''$, $u_0'' = 0$, and $c'' = c$ follows.

References

[1] Lakshminarayana B 1996 *Fluid Dynamics and Heat Transfer of Turbomachinery*, John Wiley & Sons

[2] Chorin A J 1967 *J. Comput. Phys.* **2** 12
[3] Patankar S 1980 *Numerical Heat Transfer and Fluid Flow*, McGraw-Hill, New York
[4] Beam R M and Warming R F 1976 *J. Comput. Phys.* **22** 87
[5] Jameson A, Schmidt W and Turkel E 1981 *AIAA Paper* **81−1259**
[6] Subramanian S V and Bozzola R 1987 *AIAA Paper* **87–1314**
[7] Chima R V and Yokota J W 1988 *NASA Rep.* **TM-100878**
[8] Guerra J and Gustafsson B 1986 *J. Comput. Phys.* **63** 377
[9] Rehm R and Baum H 1978 *Journal of Research of the National Bureau of Standards* **83** 297
[10] Choi D and Merkle C 1985 *AIAA J.* **23** (3) 390
[11] Leer B v, Lee W T and Roe P 1991 *AIAA Paper* **91-1552-CP**
[12] Turkel E, Vatsa V and Radespiel R 1986 *AIAA Paper* **96-2460-CP**
[13] Weiss J and Smith W 1994 *AIAA Paper* **94–2209**
[14] Lee D, Leer B v and Lynn J F 1997 *AIAA Paper* **97−2024**
[15] Merkle C L, Venkateswaran S and Deshpande M 1995 *Progress and Challenges in CFD Methods and Algorithms AGARD-CP-578*, pp. 20.1–20.10
[16] Merz R, Krückels J, Mayer J F and Stetter H 1995 *ASME Paper* **95-GT-76**
[17] Jung A R, Mayer J F and Stetter H 1997 *ASME Paper* **97-GT-94**
[18] Darmofal D L 1998 *Computational Fluid Dynamics '98*, (ed.) Papailiou K D, Tsahalis D, Périaux J and Knörzer D, ECCOMAS, Wiley & Sons
[19] Merkle C L, Sullivan J A, Buelow P E O and Venkatswaran S 1998 *AIAA J.* **36** (4) 515
[20] Giles M B 1988 *Rep. MIT, Computational Fluid Dynamics Laboratory* **TR-88-1**
[21] Saxer A P and Giles M B 1993 *AIAA J. Propulsion and Power* **9** (2) 263
[22] Merz R 1998 *Entwicklung eines Mehrgitterverfahrens zur numerischen Lösung der dreidimensionalen, kompressiblen Navier-Stokes-Gleichungen in mehrstufigen Turbomaschinen*, Dissertation, Universität Stuttgart, Institut für Thermische Strömungsmaschinen und Maschinenlaboratorium
[23] Baldwin B S and Lomax H 1978 *AIAA Paper* **78–257**
[24] Stetter H, Pfost H, Giboni A and Anker J E 2000 *FVV-Heft* **R 509**
[25] Buelow P E O 1998 *Preconditioning Methods at the Propulsion Engineering Center*, Penn State University
[26] Merkle C L 1995 *Computational Fluid Dynamics Review*, ed. Hafez M, Oshima K, Wiley, Chichester, England, pp. 419–436
[27] Venkateswaran S and Merkle L 1999 *VKI LS* 1999-03
[28] Weiss J, Maruszewski J and Smith W 1999 *AIAA J.* **37** (1) 29
[29] Radespiel R and Rossow C 1987 *Rep. DFVLR-IB* **129-87/40**
[30] Martinelli L 1987 *Calculations of Viscous Flows with a Multigrid Method*, PhD Thesis, MAE Department, Princeton University
[31] Radespiel R, Rossow C and Swanson R C 1989 *AIAA Paper* **89–1953**
[32] Lee D 1996 *Local Preconditioning of the Euler and Navier-Stokes Equations*, PhD Thesis, University of Michigan
[33] Stetter H, Pfost H, Peters P, Lerner C, Mayer J F, Giboni A, Breisig V and Anker J E 2001 *FVV-Heft* **706**
[34] Radespiel R and Swanson R C 1989 *AIAA Paper* **89–548**
[35] Saxer A P 1992 *A Numerical Analysis of 3-D Inviscid Stator/Rotor Interactions Using Non-Reflecting Boundary Conditions* PhD Thesis, MIT Gas Turbine Laboratory
[36] Stetter H, Jung A R and Mayer J F 1996 *Proc. IMechE Sem. Latest Advances in the Aerodynamics of Turbomachinery*, S461, Rugby, UK
[37] Darmofal D L, Moinier P and Giles M B 2000 *J. Comput. Phys.* **160** (1) 369
[38] Turkel E 1987 *J. Comput. Phys.* **72** 277
[39] Rizzi A and Viviand H 1981 *Notes on Numerical Fluid Mechanics GAMM Workshop*
[40] Volpe G 1993 *AIAA J.* **31** (1) 49
[41] Anker J E, Mayer J F and Stetter H 2001 *Proc. 4th European Conference on Turbomachinery, Fluid Dynamics and Thermodynamics*, Florence, Italy, pp. 641–652